



HAL
open science

Rocking response of inverted pendulum structures under blast loading

Filippo Masi, Ioannis Stefanou, Paolo Vannucci, Victor Maffi-Berthier

► To cite this version:

Filippo Masi, Ioannis Stefanou, Paolo Vannucci, Victor Maffi-Berthier. Rocking response of inverted pendulum structures under blast loading. *International Journal of Mechanical Sciences*, 2019, 157-158, pp.833-848. 10.1016/j.ijmecsci.2019.05.024 . hal-02132167

HAL Id: hal-02132167

<https://hal.science/hal-02132167>

Submitted on 16 May 2019

HAL is a multi-disciplinary open access archive for the deposit and dissemination of scientific research documents, whether they are published or not. The documents may come from teaching and research institutions in France or abroad, or from public or private research centers.

L'archive ouverte pluridisciplinaire **HAL**, est destinée au dépôt et à la diffusion de documents scientifiques de niveau recherche, publiés ou non, émanant des établissements d'enseignement et de recherche français ou étrangers, des laboratoires publics ou privés.

Rocking response of inverted pendulum structures under blast loading

Filippo Masi^{a,b}, Ioannis Stefanou^{a,*}, Paolo Vannucci^c, Victor Maffi-Berthier^b

^a*Laboratoire Navier, UMR 8205, École des Ponts, IFSTTAR, CNRS, UPE,
6-8 avenue Blaise Pascal, F-77455, Champs-sur-Marne, France.*

^b*Ingérop Conseil et Ingénierie,
18 rue des Deux Gares, F-92500, Rueil-Malmaison, France.*

^c*LMV, UMR 8100, Université de Versailles et Saint-Quentin,
55 avenue de Paris, F-78035, Versailles, France.*

We investigate the dynamics of inverted pendulum structures under fast-dynamic excitations arising from an explosion. We model blast actions using established empirical models and best-fit interpolations of existing experimental tests. We focus attention on pure rocking response mechanisms. We present moment balance equations and overturning conditions. Inspired by previous works in the frame of earthquake engineering, we derive new analytical, closed-form solutions for the rocking response and the overturning domain of slender blocks due to explosions.

The analytical findings and assumptions are validated through existing experimental tests and detailed three-dimensional numerical simulations, which consider the full interaction between the blast waves and the structure. We show that unilateral rocking response and overturning are predominant mechanisms compared to sliding and up-lifting.

Finally, we develop design charts to be used as a straightforward decision making tool for determining the critical stand-off distance between the explosive source and the target in order to prevent overturning. Our model can be easily applied for the design of protective devices to preserve artefacts, secure buildings and humans, as well as for devising energy absorbing systems based on rocking.

Keywords: Blast waves; Rocking motion; Inverted pendulum; Fluid-structure interaction; Overturning; Safety design.

*Corresponding author.

Email addresses: filippo.masi@enpc.fr (Filippo Masi), ioannis.stefanou@enpc.fr (Ioannis Stefanou), paolo.vannucci@uvsq.fr (Paolo Vannucci), victor.maffi-berthier@ingerop.com (Victor Maffi-Berthier)

Nomenclature

Blast parameters		Block's parameters	
d	exponential decay coefficient	α	° slenderness angle
i_{r+}, i_{r-}	MPa-ms positive and negative reflected impulses	ρ	kg m ⁻³ density
P_o	MPa ambient hydrostatic pressure	φ	° friction angle
P_{ro}, P_{ro-}	MPa peak of the over- and under-pressure	$2b$	m width
P_{r+}, P_{r-}	MPa time-history of the over- and under-pressure	g	m s ⁻² gravitational acceleration
R	m stand-off distance	$2h$	m height
t_A	ms arrival time	m	kg mass
t_o, t_{o-}	ms positive and negative phase durations	r	m slenderness length
W	kg TNT equivalent explosive weight	S	m ² front surface
$Z = R/\sqrt[3]{W}$	m/kg ^{1/3} Hopkinson-Cranz's scaled distance	$2w$	m depth
		\mathcal{I}_o	kg m ² moment of inertia
Response parameters		Dimensionless parameters	
θ	° rotation angle	ϕ	rotation angle
q	s ⁻¹ frequency parameter	τ	time
s	m ^{1/2} kg ^{-1/2} load parameter	τ_o, τ_{o-}	blast phase durations
t	ms time	$\chi, \bar{\chi}$	rocking and stabilising moment
		p_+, p_-	time-history of the over- and under-pressure
		$R^{\ddagger}, R^{\ddagger}$	critical distances for overturning
		$R_{num}^{\ddagger}, R_{FSI}^{\ddagger}$	numerical critical distance for overturning

1. Introduction

The dynamic behaviour of inverted pendulum structures under blast and high-rate actions is studied herein. Our modelling approach is analytical and focuses on providing closed form solutions. The most important physics of the problem are considered in order to describe the dominant features of the rocking motion due to blast waves. This is accomplished through adequate modelling assumptions, which allow the mathematical treatment of the system and the identification of the dominant parameters that pilot the dynamic behaviour and failure. Failure is defined here as the limit state where overturning (toppling) happens.

The modelling of inverted pendulum structures involves several difficulties. In particular, the inherent non-linearity and the unilateral contact conditions at the base of the inverted pendulum (rocking) make the dynamics of the system much different from the classical single- or multi-degree-of-freedom harmonic oscillators [1].

The problem of rocking attracts significant scientific research, mostly in the domain of earthquake engineering (construction of bridges, seismic isolation, masonry structures, historical monuments, etc.). We refer, for instance, to the seminal works of Omori [2, 3] and especially to the investigations of Housner [4], who was the first to study the response of a rigid, free-standing block subjected to constant and square pulse seismic (ground) accelerations. Zhang and Makris [5] investigated the overturning of a rigid block under trigonometric pulses and, more recently, Voyagaki et al. [6] studied rocking for time-symmetrical pulses of various shapes. In the same framework, Dimitrakopoulos and DeJong [7] provided useful insight on the dynamic response of a rocking block under finite-duration actions, revisiting the subject via the identification of self-similarity laws both for slender and non-slender blocks. The rocking response of structures has been also studied experimentally, e.g. [8, 9]. Peña et al. [8] investigated through shaking table tests the rocking response under free vibration, harmonic and random motions of the base and compared the test results with analytical and numerical approaches.

Interest has been also shown in the effects of blast induced ground shocks [10, 11]. Hao and Zhou [11] investigated the response of a rigid block under vertical and horizontal ground shocks. Explosion induced ground shocks are generally characterized by higher frequency content, larger amplitude, and shorter period with respect to earthquake motion. If the peak vertical ground acceleration due to ground shocks is substantially higher than the gravitational one, un-anchored rigid structures may fly into the air. We record

that in relatively far-field explosions the contribution of ground shocks is generally negligible with respect to the air-blast shock, see e.g. [12, 13, 14], where uplifting due to vertical ground accelerations is unlikely.

Our developments take root in the existing knowledge and theory of inverted pendulum structures subjected to earthquake loading and extend them to non-symmetrical pulses provoked by blast waves. We model blast actions using well-established empirical models accounting for both the positive and the negative phase of the blast pressure. Moment balance equations and overturning conditions are presented and used to determine the critical (minimum) stand-off distance between the source and the target to prevent toppling. This is accomplished by deriving new analytical, closed-form solutions, which lead to the identification of the central and dominant dimensionless parameters that govern the dynamical behaviour of the system. These dimensional parameters improve and extend the current understanding of rocking due to blasts (cf. [10, 11, 12, 13, 14, 15, 16, 17]) and lead to fundamental insights for design. Moreover, they can be helpful to conceive in-scale experimental tests focusing on overturning of (slender) blocks at the loading rates under study. Notice that performing blast experiments either in reduced [17] or in full scale [12] presents many difficulties, due to the nature of the loading action (e.g. need of specialized personnel, risks, measuring devices, repeatability, uncertainties etc.).

Contrary to earthquake actions, the excitation due to explosions presents additional complexity. This is not only because of the ultra-high rates involved—the characteristic time of a blast is of several milliseconds instead of $\approx 1 \div 10$ s for earthquakes—but also due to several phenomena related to wave propagation and fluid-structure interaction (e.g. diffraction, rarefaction, reflections, damage etc.). The effect of these phenomena on our modelling assumptions is extensively discussed in the manuscript. More specifically, the predictions of our analytical model are compared to detailed numerical analyses that consider the above mentioned phenomena, a combined sliding/rocking behaviour, and the possibility of uplifting (flight mode). The numerical analyses are three-dimensional, they benefit from the well-established balloon analogue [18] for modelling the explosive source and they are based on a Coupled Eulerian-Lagrangian (CEL) scheme for modelling the propagation of shock waves and their interaction with the rocking block. It is worth emphasizing that a complete 3D fluid-structure interaction of shock waves with all sides of the block is considered in order to assess the validity of our modelling assumptions and simplifications. Finally, the results of our analytical model are confirmed by comparisons with existing experimental results [17, 12].

Engineering applications of the present study can be found in several domains. For instance, our analyses can be used for protecting un-anchored equipment and museum (slender) artefacts from overturning (e.g. statues), securing historical buildings made of monolithic columns from collapse (e.g. classical Greek and Roman temples [19], [20]) and for designing barriers and blast walls to protect existing buildings, assets and humans. Finally, our analysis can be used for conceiving energy absorbing systems based on rocking.

The paper is structured as follows. In Section 2 we present the main assumptions of our modelling approach regarding the dynamics of the system and the considered blast actions. Our simplifying assumptions cover a broad spectrum of loading cases. In Section 3 we derive analytical solutions for the non-linear rocking motion and the overturning domain, by considering only the positive phase of the blast action. Then, in Section 4 we assess the influence of the negative phase, which has a significant stabilising effect as far as it concerns toppling. Detailed charts for the critical stand-off distance (i.e., the minimum distance to avoid targets overturning) are presented as a result of the analytical model. Finally, in Section 5 we investigate the accuracy and the validity of the main assumptions of our model through detailed numerical simulations and the limited experimental results that were retrieved from the literature.

2. Statement of the problem

The problem of a rigid block resting on a horizontal plane is studied based on the following assumptions (Fig. 1):

- i.* A rectangular slender, rigid block is assumed with a uniformly distributed mass m . The dimensions of the block are $2b \times 2h \times 2w$ and the radial distance from the rocking pivot point O to the centre of gravity is $r = b \sec \alpha$, where α is the slenderness angle.

- ii. The contact with the horizontal plane is assumed punctual at point O (no contact moment). Contact is considered to be unilateral. The angle of friction, φ , is assumed to be sufficiently large to prevent sliding.
- iii. The pressure load due to the explosion is exclusively applied on the front surface S (incident surface, see Fig. 1) and the blast wave is assumed to impinge all points of S at the same time (simultaneously) and with the same magnitude (uniformly). We consider the resulting load to act always horizontally and at the block's centroid as the loading pulse duration is extremely short (i.e., small inclination angle within the duration of the loading). Diffraction phenomena are neglected. The effects of induced ground shocks are also omitted [11, 14].

These simplifying assumptions are helpful for reducing the complexity of the problem and for deriving analytical, closed-form solutions. Their adequacy is explored in Section 5, where it is shown that the analytical solution represents quite well the dynamic behaviour of the system and the overturning condition. In particular, it is shown that the minimum distance that has to be assured between the explosive source and the target, such that toppling is avoided, is in good agreement and on the safety side with the one determined by the full numerical model and experimental results presented in Section 5.

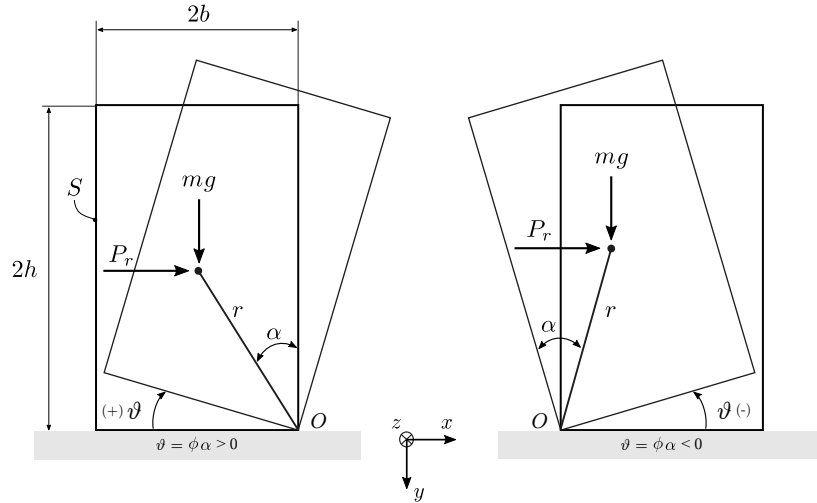


Figure 1: Configuration considered for the rocking problem: a rectangular slender, rigid block resting on a horizontal plane with uniformly distributed mass, subjected to uniform pressure load due to an explosion.

2.1. Rocking motion

Depending on the characteristics of the excitation and the properties of the friction angle, the rigid block can either slide, rock, or both. As far as it concerns the response mechanisms of pure rocking and sliding, the corresponding initiation conditions can be found from rotational and translational equilibria, respectively.

- *Rocking initiation.* Rocking initiates if the moment due to blast actions exceeds the restoring moment due to gravity. The initiation condition reads

$$\frac{S}{mg} P_{ro} \geq \tan \alpha, \quad (1)$$

where P_{ro} is the overpressure peak acting on block's front surface S (see below), and g is the gravitational acceleration.

- *Sliding initiation.* Sliding initiates when

$$\frac{S}{mg} P_{ro} \geq \tan \varphi. \quad (2)$$

For relatively slender blocks, i.e. $\alpha \leq 20^\circ$, which are of interest here, and for an angle of friction $\varphi \approx 30^\circ$ (typical value for marble to marble interfaces see for instance [21]), rocking is critical.

2.2. Blast actions

Explosion produces a blast wave of high-pressure accompanying high-temperature and supersonic expansion of gases. The abrupt increase of the pressure carried by a blast wave can produce severe structural damage. When the primary shock meets a target, it generates on it the so-called *reflected overpressure*, P_r , which is the difference between the pressure determined by the explosion increased by the reflection at target's surface and the ambient one, P_o . Figure 2 shows the schematic time variation of P_r , which is determined by the arrival time of the shock wave, t_A , the overpressure peak, P_{ro} , the positive phase duration, t_o , negative phase duration, t_{o-} , and the underpressure peak, P_{ro-} . These parameters are functions of the distance R and the explosive weight (conventionally expressed in TNT equivalent).

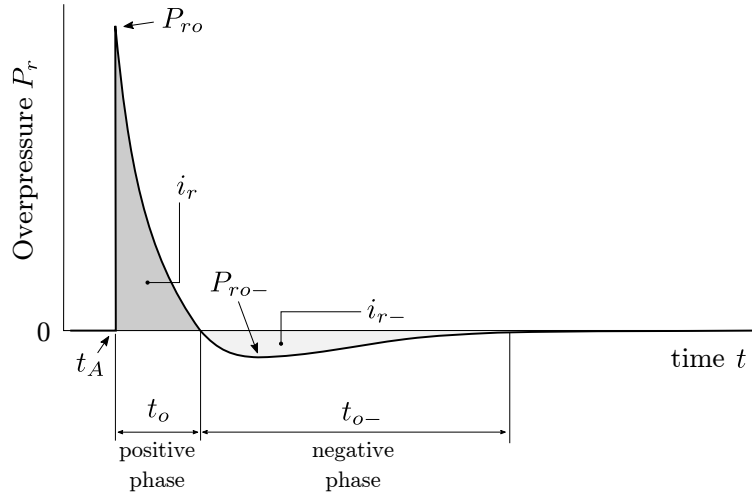


Figure 2: Time evolution of overpressure (i.e. the pressure measured relatively to the atmospheric one) due to an explosion acting on a target. The blast load is determined by the arrival time of the shock wave, t_A , the overpressure peak, P_{ro} , the positive phase duration, t_o , negative phase duration, t_{o-} , and the underpressure peak, P_{ro-} .

The simulation of a blast can be conducted by using different approaches [22, 23, 24], i.e., empirical or physics-based ones. These models are presented below.

2.2.1. Empirical models

Empirical models rely on best-fit interpolations of experimental results and mainly on those of Kingery and Bulmash [25], which allow to determine the blast parameters and pressure loading from the knowledge of the trinitrotoluene (TNT) equivalent explosive weight, W , and the Hopkinson-Cranz scaled distance,

$Z = R/\sqrt[3]{W}$ (see Appendix A). The time evolution of the positive phase of the reflected pressure is modelled with the well established *modified Friedlander equation* [26],

$$P_{r+}(t) = P_{ro} \left[\left(1 - \frac{t}{t_o}\right) \left(1 - \mathcal{H}[t - t_o]\right) \right] \exp\left(-d\frac{t}{t_o}\right), \quad (3)$$

where $\mathcal{H}[\cdot]$ denotes the Heaviside (step) function, d is the exponential decay coefficient, and t_A is taken as the origin of the time axis. The impulse i_r associated to the positive phase, which represents the area beneath the pressure curve, reads

$$i_{r+} = \int_0^{t_o} P_{r+} dt = [e^{-d} + d - 1] \frac{P_{ro} t_o}{d^2}, \quad (4)$$

The above equation allows to determine the exponential decay coefficient, d , by equating it with the best-fit interpolation of i_r from experiments (see Appendix A).

The negative phase is modelled with the so-called cubic approximation [27], namely

$$P_{r-}(t) = P_{ro-} \left(\frac{27}{4} \frac{t - t_o}{t_{o-}}\right) \left(1 - \frac{t - t_o}{t_{o-}}\right)^2 \left(\mathcal{H}[t - t_o] - \mathcal{H}[t - (t_o + t_{o-})]\right). \quad (5)$$

Accordingly, the negative reflected impulse i_{r-} can be evaluated as

$$i_{r-} = \int_{t_o}^{t_o+t_{o-}} P_{r-} dt = \frac{9P_{ro-} t_{o-}}{16}, \quad (6)$$

which is computed from the best-fit interpolations of t_{o-} and P_{ro-} (see again Appendix A).

It is worth noting that Friedlander equation captures very well the positive phase of the reflected pressure as compared to extensive experimental data. However, for the negative phase of the reflected pressure there is not a universal, established best-fit expression. Here we follow the work of Rigby et al. [28] and we use the cubic approximation, which gives a reasonable agreement with experimental evidence.

2.2.2. Numerical physics-based models

Physics-based, numerical approaches allow a rather detailed description of the main features of the blast phenomenon with, of course, an increased calculation cost. They rely on the definition of two domains: the explosive charge and the surrounding air. Through numerical simulations, detonation, propagation of shock waves and their interaction with deformable structures can be efficiently modelled with a Coupled Eulerian-Lagrangian (CEL) scheme.

Air is commonly considered as an ideal gas in these simulations. Explosive is usually modelled with the empirical JWL equation of state (Jones, Wilkins, and Lee [29, 30, 31]), which relies on a steady-state ideal detonation model [32, 33]. An alternative, simplified model for generating the blast wave is the so-called *balloon analogue* [34]. This approach replaces the solid explosive charge with an energetically equivalent sphere of compressed air, resulting in reduced calculation cost compared to the JWL. Moreover, this approach has been proved to be in good agreement with experimental tests and numerical analyses [23, 18], and this is why we use it in Section 5.

3. Rocking response to an explosion

First we solely account for the positive phase using the empirical relation of Friedlander. The negative phase is expected to have a stabilising effect on the rocking response and, therefore, its influence is studied separately in the next section. In all cases, the explosive source is considered to be (very) close to the ground (surface burst).

3.1. Equation of motion

The moment balance around the rocking pivot point gives the equation of motion

$$\left. \begin{aligned} \mathcal{I}_o \ddot{\theta} + mgr \sin(\alpha - \theta) &= SrP_r \cos(\alpha - \theta), & \theta(t) > 0, \\ \mathcal{I}_o \ddot{\theta} + mgr \sin(-\alpha - \theta) &= SrP_r \cos(-\alpha - \theta), & \theta(t) < 0, \end{aligned} \right\} \quad (7)$$

where $\mathcal{I}_o = (4/3)mr^2$ is the moment of inertia with respect to the pivot point, $\theta = \theta(t)$ is the inclination angle, and $P_r = P_{r+}(t)$ is the loading which is given by the Friedlander equation (3) as mentioned above. Introducing the frequency parameter q , and the load parameter, s , the above equations can be rearranged into

$$\frac{\ddot{\theta}}{q^2} = -\sin[\alpha \operatorname{sgn}(\theta) - \theta] + \frac{s^2}{q^2} P_{ro} p \cos[\alpha \operatorname{sgn}(\theta) - \theta], \quad (8)$$

where $\operatorname{sgn}(\cdot)$ denotes the signum function and

$$\begin{aligned} q &= \sqrt{\frac{mgr}{\mathcal{I}_o}} = \sqrt{\frac{3g}{4r}}, \\ s &= \sqrt{\frac{Sr}{\mathcal{I}_o}} = \frac{1}{2} \sqrt{\frac{3}{2b\rho r}}, \\ p &= \frac{P_r}{P_{ro}}, \end{aligned} \quad (9)$$

with ρ the material density.

3.1.1. Dimensionless form of governing equations

Using the dimensionless angle of rotation $\phi = \theta/\alpha$ and the normalized time $\tau = qt$ we obtain

$$\ddot{\phi} = -\frac{1}{\alpha} \sin[\alpha (\operatorname{sgn}(\phi) - \phi)] + \chi p \cos[\alpha (\operatorname{sgn}(\phi) - \phi)], \quad (10)$$

where χ represents the normalized rocking moment, i.e., the ratio between the moment due to the blast load and the restoring moment due to gravity, p_+ the normalized Friedlander time-history, and τ_o the ratio between the characteristic time of the load and the time parameter, T , related to the response of the rigid block.

$$\begin{aligned} \chi &= \frac{s^2 P_{ro}}{q^2 \alpha} = \frac{1}{2\rho bg} \frac{P_{ro}}{\alpha}, \\ p_+ &= \left[\left(1 - \frac{\tau}{\tau_o}\right) \left(1 - \mathcal{H}[\tau - \tau_o]\right) \right] e^{-d\frac{\tau}{\tau_o}}, \\ \tau_o &= qt_o = \frac{t_o}{T}. \end{aligned} \quad (11)$$

3.1.2. Analytical solution for slender blocks

For tall, slender blocks, angles θ and α are small and the equation of motion (10) can be linearised using the first-order approximations $\sin(\cdot) \cong \cdot$ and $\cos(\cdot) \cong 1$

$$\ddot{\phi} = \phi + \chi p_+ - \operatorname{sgn}(\phi). \quad (12)$$

Notice that under this normalization the rocking initiation condition, Eq. (1), reads $\chi \geq 1$.

As the load is acting always on the same direction (positive), a unilateral response mechanism is expected. Here we focus on overturning, thus we restrict expression (12) to positive angles only,

$$\ddot{\phi} = \phi + \chi p_+ - 1. \quad (13)$$

Initially the block is at rest ($\dot{\phi}(0) = 0$, $\phi(0) = 0$). Equation (13) admits a close form solution, whose complete mathematical expression is given in Appendix B.

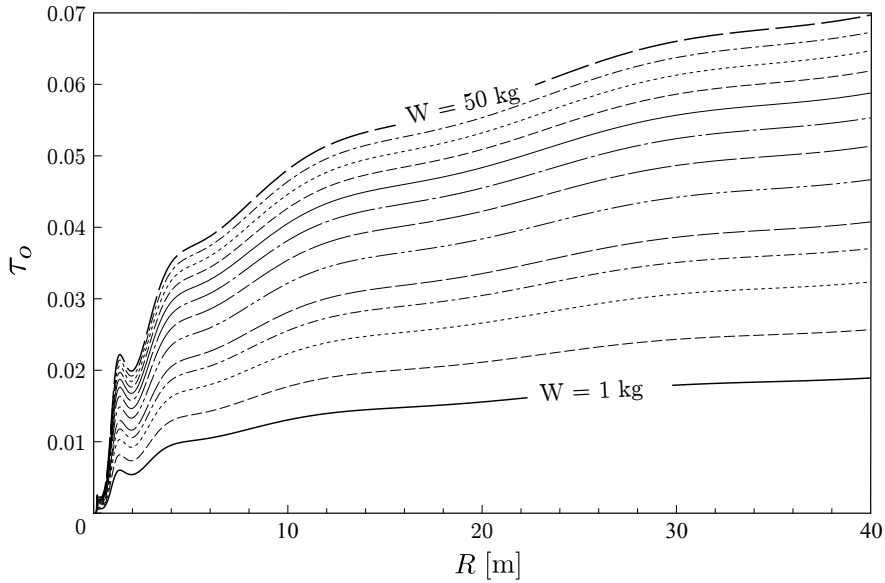


Figure 3: Normalized time, $\tau_o = t_o/T$ in function of the stand-off distance, R , for different explosive quantities, W , in equivalent TNT weight. The ratio between the characteristic time of the blast load, t_o , and the time parameter, T , related to the dynamic, rocking, response of the rigid block is small for blocks of centrimetric scale or larger.

Notice that the characteristic time parameter, T , of blocks of centrimetric scale or larger, is much higher than the characteristic time of blast loads t_o and, therefore, $\tau_o \ll 1$. Figure 3 shows τ_o with respect to the explosive weight, W , and the stand-off distance, R . For instance, if we consider $h = 1$ m, 1 kg of TNT and a stand-off distance $R = 10$ m, $\tau_o \approx 0.01$, i.e., the positive phase duration, t_o , is two orders of magnitude smaller than T . Indeed, a $\tau \approx 1$ for the same values of W and R would actually correspond to a block with a height of ≈ 0.33 mm, which is too small for the applications that we focus on in the current paper.

3.2. Overturning domain

For unilateral excitations, overturning happens when the rocking angle $\theta \geq \alpha$ or, equivalently, when $\phi \geq 1$. The overturning condition can be found by equating the total work done by the blast load to the difference in potential energy between positions $\theta = \alpha$ and $\theta = 0$ (see also Housner, [4]):

$$\int_0^\infty rSP_{\tau_o} p \dot{\theta} \cos(\alpha - \theta) dt \geq mgr(1 - \cos \alpha). \quad (14)$$

Noticing that $p(t \geq t_o) = 0$ and rearranging the inequality in terms of the non-dimensional rocking angle and normalized time, one obtains

$$\alpha r S P_{r_o} \int_0^{\tau_o} p_+ \dot{\phi} \cos[\alpha(1-\phi)] d\tau \geq mgr(1 - \cos \alpha). \quad (15)$$

Applying further the mean-value theorem, Eq. (15) becomes

$$\frac{\alpha^2 \cos[\alpha(1-\tilde{\phi})]}{1 - \cos \alpha} I \chi \geq 1, \quad (16)$$

$$I = \int_0^{\tau_o} p_+ \dot{\phi} d\tau,$$

where $0 < \tilde{\phi} \leq 1$.

For slender blocks, the power series expansion at the first order gives $(1 - \cos \alpha) \cong \alpha^2/2$ and $\cos[\alpha(1-\tilde{\phi})] \cong 1$, hence the overturning condition simply becomes

$$2I\chi \geq 1, \quad (17)$$

The left-hand side term in inequality (17) represents the non-dimensional overturning moment.

Figure 4 shows the dimensionless rocking and overturning moments as functions of the stand-off distance, R , for an explosion of 1 kg of TNT. The rocking moment, χ , expresses the condition for rocking initiation ($\chi \geq 1$), while the overturning moment the condition for overturning ($2I\chi \geq 1$). We observe that the minimum stand-off distance to avoid overturning is 0.6 m. For $R \geq 35$ m, rocking is not initiated at all.

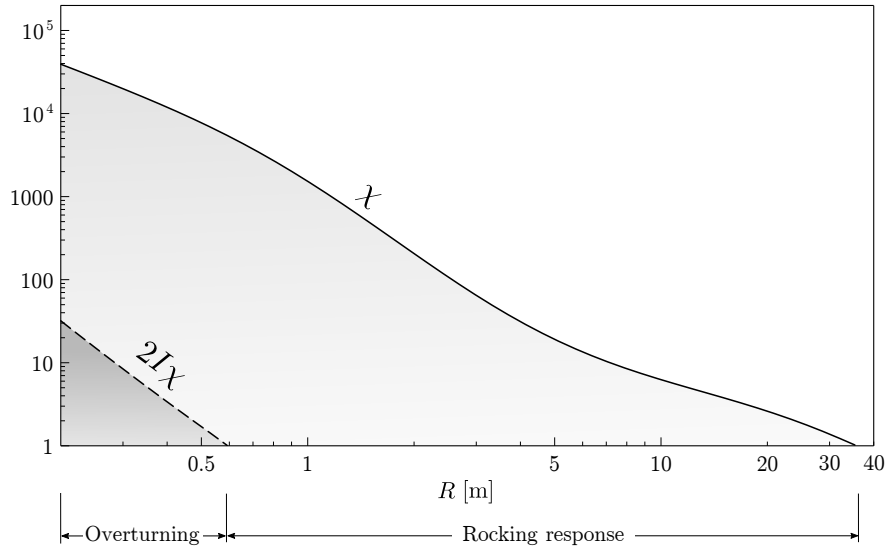


Figure 4: Rocking initiation and overturning conditions for a block with $h = 1$ m, $\rho = 2000$ kg/m³, and $\alpha = 20^\circ$, subjected to $W = 1$ kg at various stand-off distances, R . The rocking moment, χ , expresses the condition for rocking initiation ($\chi \geq 1$), while the overturning moment the condition for overturning ($2I\chi \geq 1$).

It is worth comparing the overturning condition from the linearised equations of motion with the one from the non-linear ones. Taking the ratio between the non-dimensional overturning moments in expression

(16) and (17) and further considering angles $\alpha \leq 20^\circ$, we obtain

$$\frac{\text{non-linear overturning condition}}{\text{linear overturning condition}} = 1 - \frac{1}{2} \left[\alpha \left(1 - \tilde{\phi} \right) \right]^2 \leq 1. \quad (18)$$

Therefore, the linearised overturning condition is a lower bound of the *exact* one. The ratio is usually higher than 0.95 for blocks with $\alpha \leq 20^\circ$ and does not drop under 0.80 for $\alpha < 40^\circ$ (see also [6]).

3.3. *Minimum stand-off distance*

Using the overturning condition ($2I\chi = 1$) we can determine the minimum required distance between the explosive source and the target, R^\sharp , in order to avoid toppling. Figure 5 shows the contours of the critical distance R^\sharp for different slenderness angles, block heights, densities, and explosive quantities.

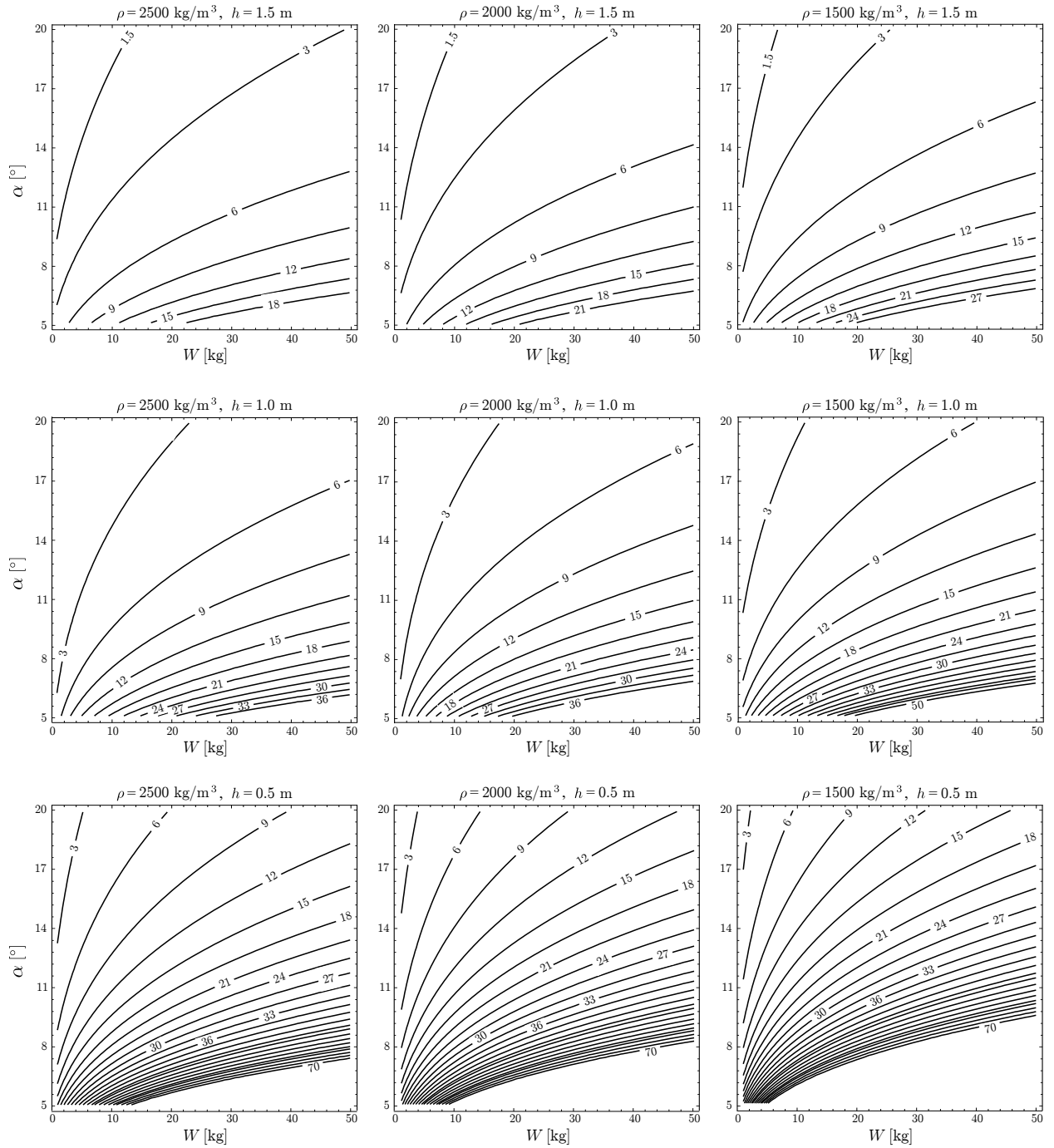


Figure 5: Contours of the critical stand-off distance, i.e., the minimum required distance between the explosive source and the rigid target, R^{\sharp} , in order to avoid toppling. For $\rho = 2500$ (left column), 2000 (centre column), 1500 kg/m^3 (right column), heights $h = 1.5$ (top row), 1.0 (centre row), 0.5 m (bottom row), R^{\sharp} is plotted as a function of the explosive quantity, W , and slenderness, α .

4. Influence of the negative phase

In this section attention is focused on the influence of the negative phase on the response mechanisms and the overturning criterion. We represent the positive phase with Friedlander equation as above, but in this case the negative phase is also considered (see paragraph 2.2.1).

Equations (10) and (13) become respectively

$$\ddot{\phi} = -\frac{1}{\alpha} \tan [\alpha (\operatorname{sgn}(\phi) - \phi)] + \chi p_+ - \bar{\chi} p_-, \quad (19)$$

and

$$\dot{\phi} = \phi + \chi p_+ - \bar{\chi} p_- - \operatorname{sgn}(\phi). \quad (20)$$

$\bar{\chi}$ is the dimensionless blast stabilising moment, i.e., a negative pressure component, which has a restoring role, p_- the normalized negative time-history, and τ_{o-} the ratio between the characteristic time of the negative phase and the time parameter of the rigid block:

$$\begin{aligned} \bar{\chi} &= \frac{s^2 P_{ro-}}{q^2 \alpha}, \\ p_- &= \left(\frac{27}{4} \frac{\tau - \tau_o}{\tau_{o-}} \right) \left(1 - \frac{\tau - \tau_o}{\tau_{o-}} \right)^2 \left(\mathcal{H}[\tau - \tau_o] - \mathcal{H}[\tau - (\tau_o + \tau_{o-})] \right), \\ \tau_{o-} &= q t_{o-} = \frac{t_{o-}}{T}. \end{aligned} \quad (21)$$

Equation (20) admits a closed-form solution under the assumption of small slenderness angles. The solutions $\phi, \dot{\phi}$ are given in Appendix B.

The negative phase plays a significant role on the response mechanism. In Figure 6 we present the angular displacement and velocity as solutions of Eq.s (12) and (20). Perfectly plastic impact is considered. The plots display the response due to a 10 kg TNT explosive charge at varying stand-off distance and for a block with $\alpha = 15^\circ$, $\rho = 2000 \text{ kg/m}^3$ and $h = 1 \text{ m}$. The negative phase clearly limits the amplitude of the rocking angle since the suction component of the blast load acts as a restoring moment, see Eq. (19).

Figures 7 and 8 depict the trajectories $(\phi, \dot{\phi})$ in the phase space. The phase portraits highlight the pulse nature of blast loads. Notice that the duration of the positive phase, t_o , is extremely short and in some cases it may be replaced by an instantaneous increment of the angular velocity $\dot{\phi}$ at $\phi = 0$, as suggested in [12].

Figure 8 shows the important role of the negative phase, which decreases the angular velocity $\dot{\phi}$ and stabilizes the system. Contrary to the positive phase, the negative one can be hardly simplified by a jump discontinuity of $\dot{\phi}$.

4.1. Overturning domain and minimum stand-off distance

The overturning condition can be written taking advantage of Eq. (14) and updating the work done by the external loads in order to consider the negative phase, as follows

$$\frac{\alpha^2 \cos [\alpha(1 - \tilde{\phi})]}{1 - \cos \alpha} (I\chi - \bar{I}\bar{\chi}) \geq 1, \quad (22)$$

where

$$I = \int_0^{\tau_o} p_+ \dot{\phi} d\tau \quad \text{and} \quad \bar{I} = \int_{\tau_o}^{\tau_o + \tau_{o-}} p_- \dot{\phi} d\tau, \quad (23)$$

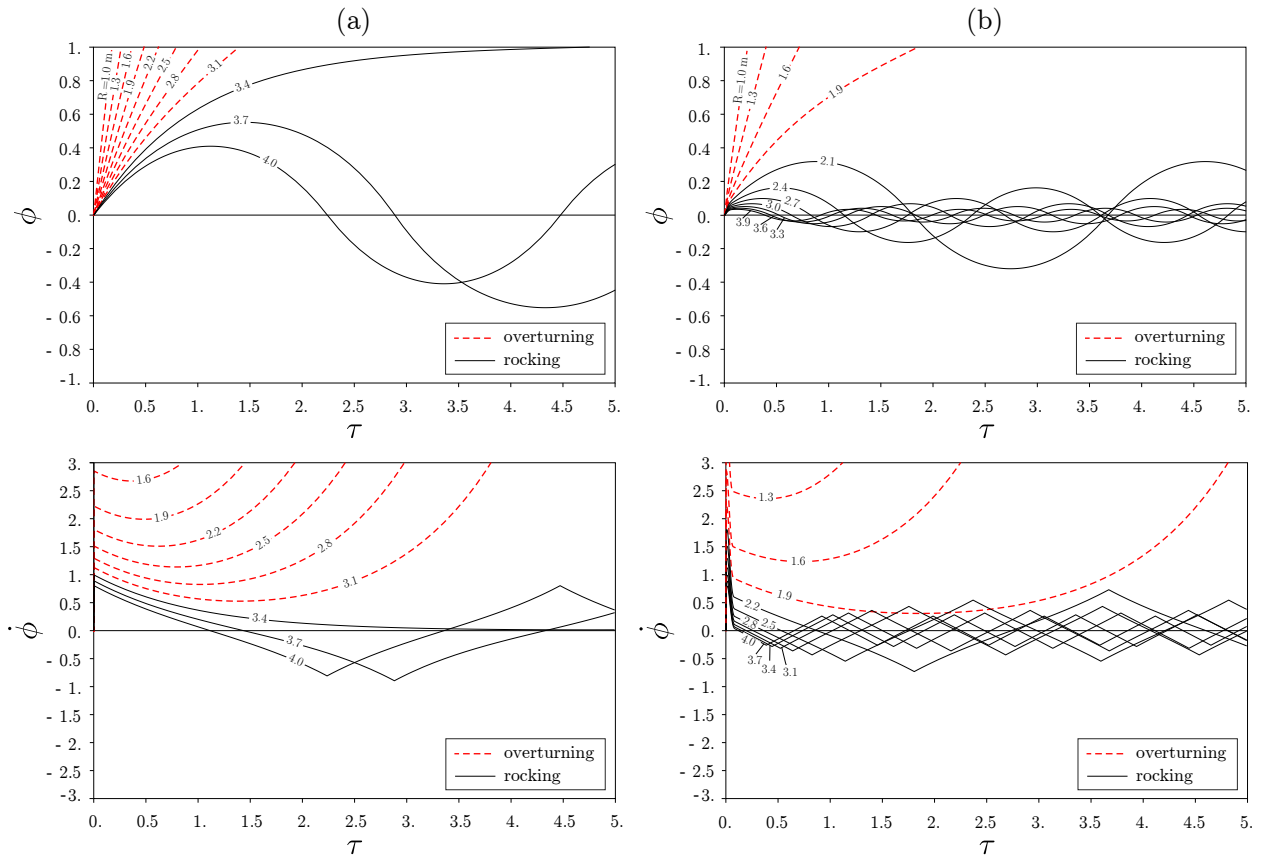


Figure 6: Normalized inclination angle, ϕ , and angular velocity, $\dot{\phi}$, of the rocking block considering (a) only the positive phase of the blast wave, Eq. (12), and (b) accounting for both positive and negative blast phases, Eq. (20). The plots refer to a TNT explosive weight $W = 10$ kg and a rigid target with $\alpha = 15^\circ$, $h = 1$ m, $\rho = 2000$ kg/m³, for stand-off distances $R \in [1, 4]$ m. Red dashed curves indicate overturning.

For slender blocks, equation (23) is simplified to

$$2(I\chi - \bar{I}\bar{\chi}) \geq 1. \quad (24)$$

The required minimum distance between an explosive source W and a block in order to avoid toppling, is here denoted with R^\natural and is retrieved by setting $(2(I\chi + \bar{I}\bar{\chi}) = 1)$. In Figure 9 we present the contours of the critical stand-off distance R^\natural , for different values of ρ , h , W and α . It should be emphasized that the negative phase *de novo* engenders a considerable stabilising effect.

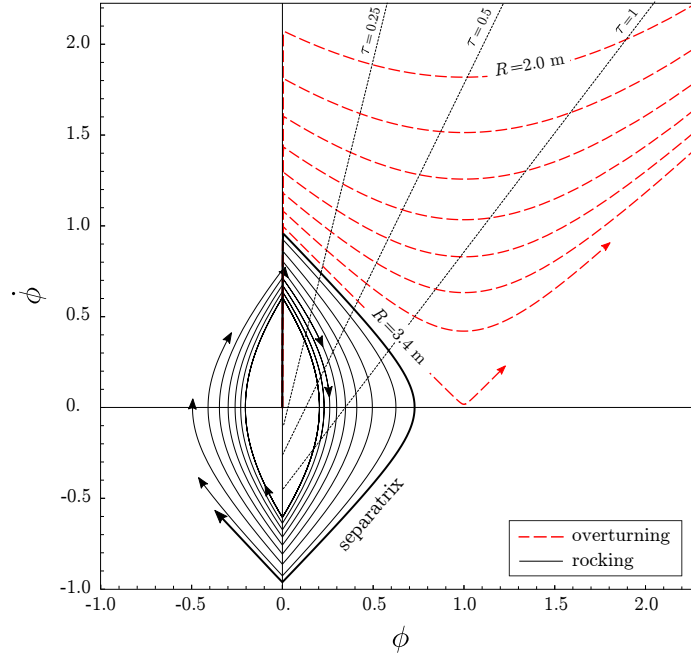


Figure 7: Phase space $(\phi, \dot{\phi})$ considering only the blast positive phase. In this plot, the TNT explosive weight is $W = 10$ kg and the rigid target has $\alpha = 15^\circ$, $h = 1$ m, $\rho = 2000$ kg/m³. Different values of the stand-off distance are considered, $R \in [2, 5]$ m. Red dashed curves correspond to overturning. Dotted lines represent contours of the dimensionless time, τ_o .

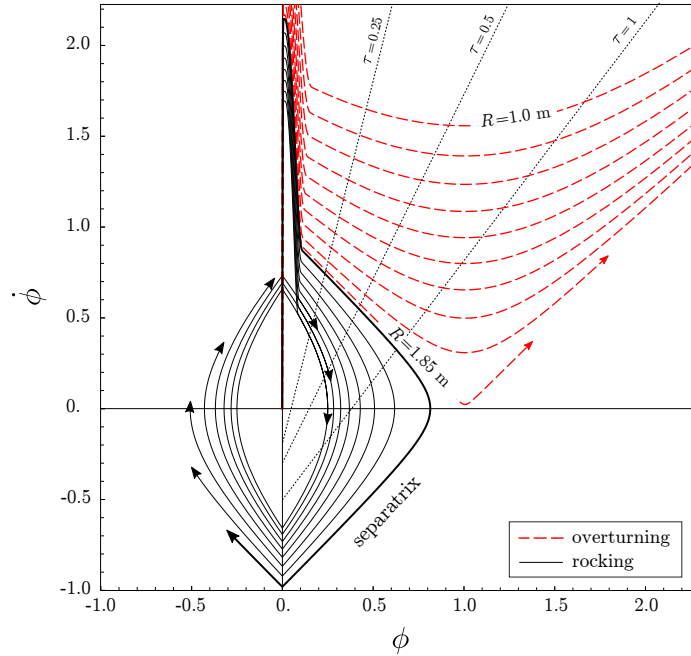


Figure 8: Phase space $(\phi, \dot{\phi})$ considering both the blast positive and negative phase, see Eq. (20). The TNT explosive weight is $W = 10$ kg and the rigid target has $\alpha = 15^\circ$, $h = 1$ m, $\rho = 2000$ kg/m³. Different values of the stand-off distance are considered, $R \in [1.5, 2.3]$ m. Red dashed curves correspond to overturning. Dotted lines represent contours of the dimensionless time, τ_o .

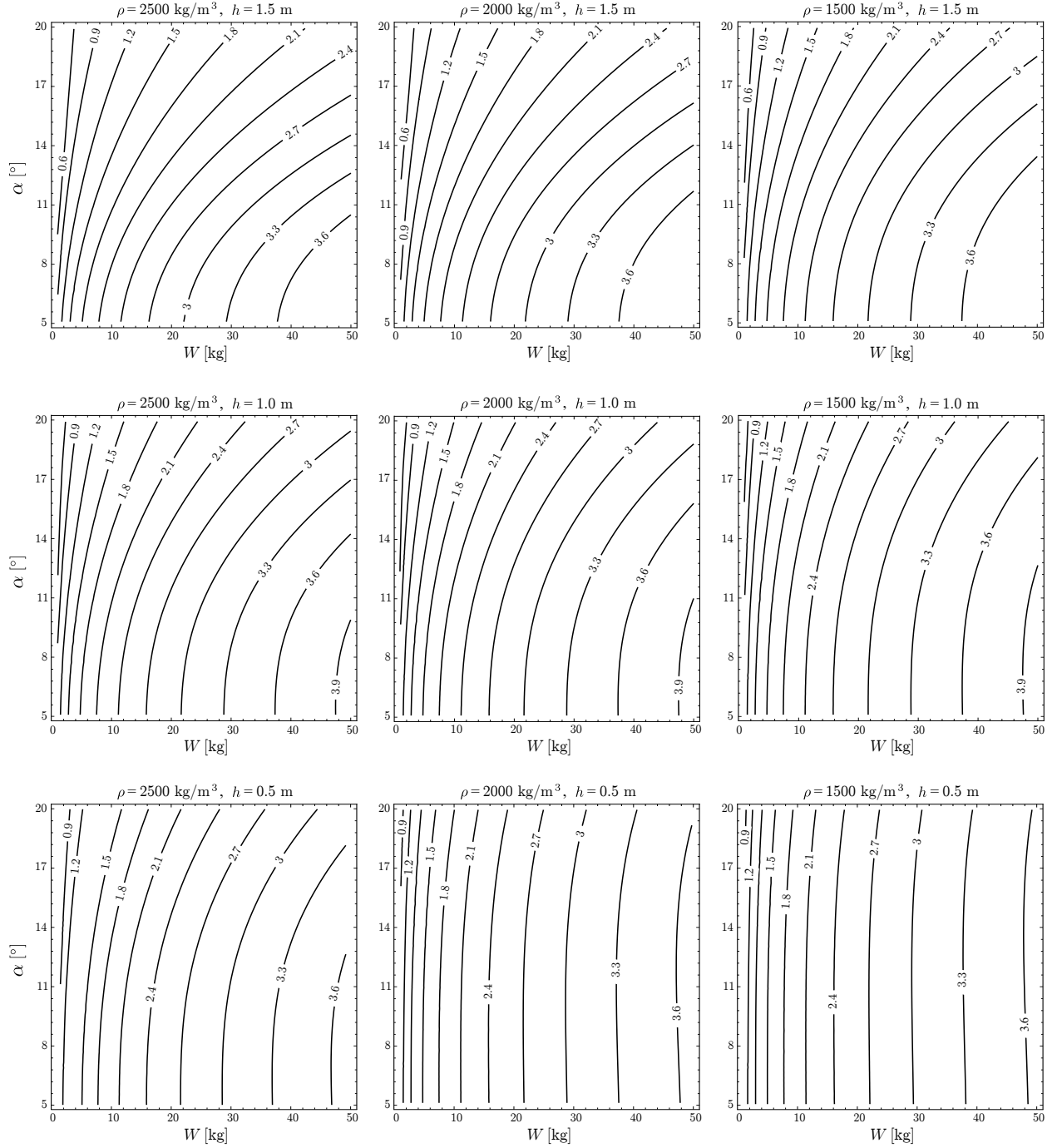


Figure 9: Contours of the critical stand-off distance, i.e., the minimum required distance between the explosive source and the rigid target, R^d , in order to avoid toppling. The effect of both positive and negative phases of the blast wave is considered. For $\rho = 2500$ (left column), 2000 (centre column), 1500 kg/m^3 (right column), heights $h = 1.5$ (top row), 1.0 (centre row), 0.5 m (bottom row), R^d is plotted as a function of the explosive quantity, W , and slenderness, α . The negative phase has a significant stabilising effect (see also Fig. 5).

5. Validation of the overturning domain

The analytical approach presented in the previous sections allowed to determine the minimum stand-off distance to prevent toppling. The calculations lead to closed-form solutions, which are useful for identifying the main factors that influence the dynamic response of the system under explosive loads. However, the aforementioned approach is based on some simplifying assumptions (see Sect. 2), whose validity is explored in the present Section.

Of interest here is the minimum stand-off distance, which is a central design quantity for protective measures. This quantity is first validated through numerical analyses that introduce more physics into the blast wave loading, its interaction with the rocking block, and the full dynamic response of the system. Next, the predictions of our analytical model are validated through available experimental results.

First we explore the validity of assumptions (i) and (ii) of Section 2. In other words, we quantify *a*) the linearisation of the equations of motion (see also paragraph 3.2), and *b*) the effect of combined sliding, rocking, and uplift (flight mode). We consider Coulomb friction at the interface of the block with the rigid base, with an angle of friction equal to $\varphi = 35^\circ$, which is common for many geomaterials (concrete, marble, stone etc.). Blast loads are applied as in Section 4, relying on the best-fit interpolations in Appendix A. ABAQUS commercial software is used for the computations. A *hard* contact formulation is used, i.e., no penetration is allowed at the contact of the rocking block with the base [35]. The rigid base is fixed and the rigid block is free to translate along y - and x -axes, rotate around z , and uplift, see Figure 1.

It should be mentioned that our analyses are made only for rigid blocks. In the case of deformable ones, where significant dissipation is expected due to, for instance, deformability and damage, our model might underestimate the resistance of the system to overturning that allow to be on the safety side.

Next, we focus on assumption (iii) which concerns the simplifications related to the blast loads and their approximation by empirical models. In particular, we investigate the effects due to the interaction between blast waves and the rocking block. The analyses are performed again using ABAQUS software. The same modelling approach is used for the interaction of the block and the base as before. The results of this comparison are presented in paragraph 5.2, *Comparison C2*.

Finally, we validate our model with existing experimental tests of quasi-rigid (stiff) [17] and deformable targets [12] subjected to explosions. Both the overturning domain and the rocking response are compared with large-scale tests. This comparison allows us to explore the validity of our assumptions in general and, in particular, to assess the effects of explosion induced ground motions [14, 11], which the above mentioned numerical model does not account for. In accordance with [14], the aforementioned ground motions were found to have negligible effects. The results are presented in paragraph 5.3, *Comparison C3*.

5.1. Comparison C1

We investigate the minimum stand-off distance (R_{num}^{\natural}) for several combinations of slenderness angles and explosive weights. Figure 10 depicts the response of the rigid block, while Table 1 displays the comparison between the threshold range (R^{\natural}), derived in Section 4, and the one obtained from the numerical simulations (R_{num}^{\natural}). Finally, in Figure 11 we present the ratio $R_{num}^{\natural}/R^{\natural}$ as function of W .

The numerical analyses show that rocking and sliding happen together. However, for slender structures sliding is limited and rocking prevails. This justifies the no-sliding assumption. For blocks of high slenderness, sliding becomes even smaller and practically only rocking is observed. For blocks of lower slenderness, sliding has a more important effect and becomes more pronounced for increasing explosive weights. In the worst case studied here ($W = 50$ kg and $\alpha = 20^\circ$) the analytical approximation overestimates the minimum stand-off distance by approximately 25%. This is due to the fact that by increasing W , the duration of the positive phase increases (see Figs 3, 6) enhancing sliding and frictional energy dissipation (toppling is less favorable due to low slenderness). Consequently, our analytical estimation provides a close upper bound for the critical distance and, therefore, can be safely used for the design of protective measures.

Table 1: Comparison of the overturning domain between the analytical solution, R^{\natural} , and the numerical one, R_{num}^{\natural} . The rocking block has $h = 1$ m, $\rho = 2000$ kg/m³, and variable slenderness angle α . Different weights of TNT, W , are considered. Good agreement is found, being always on the safety side.

		$\alpha = 20^\circ$			$\alpha = 15^\circ$			$\alpha = 10^\circ$		
W	[kg]	10	20	50	10	20	50	10	20	50
t_o	[ms]	1.292	1.744	2.422	2.499	2.991	3.507	3.728	3.873	4.01
R^{\natural}	[m]	1.51	2.10	3.18	1.88	2.53	3.67	2.21	2.84	3.93
R_{num}^{\natural}	[m]	1.40	1.75	2.40	1.85	2.35	3.15	2.20	2.80	3.15
$\frac{R_{num}^{\natural}}{R^{\natural}}$		0.9283	0.8373	0.7547	0.9831	0.9282	0.8580	0.9965	0.9919	0.9899

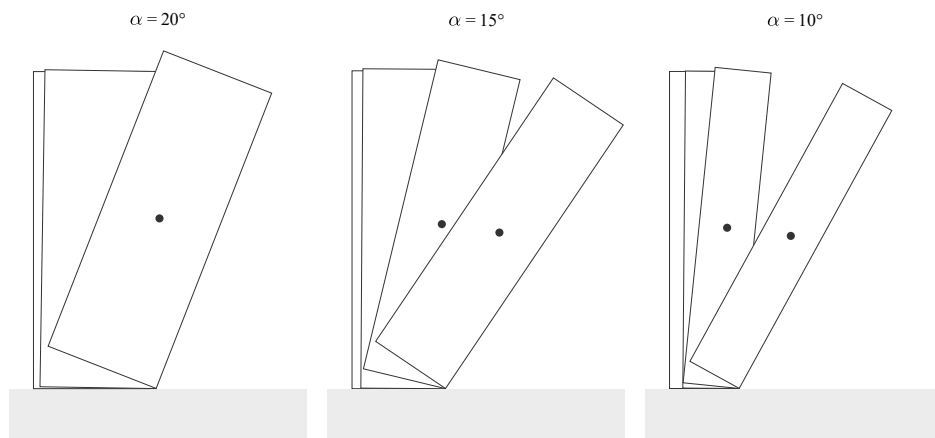


Figure 10: Response mechanism as computed by numerical simulations considering an empirical model for blast actions and allowing for sliding, rocking and uplift. The explosive quantity considered is $W = 10$ kg. The rocking block has $h = 1$ m, $\rho = 2000$ kg/m³ and slenderness angle α equal to 20° (left), 15° (center) and 10° (right). Overturning is observed with limited sliding.

5.2. Comparison C2

We account for three-dimensional Fluid-Structure Interactions (FSI) with a CEL approach: the balloon analogue models the explosive source and air is assumed as an ideal gas. The material parameters for the constitutive laws of the balloon are those detailed in [18] (p. 645, model #6). Figure 12 displays the geometry of the whole domain. We impose symmetry along the $x - y$ plane and non-reflecting boundary conditions at the other faces. To ensure mesh convergence, the Eulerian domain is discretized with 8-node linear hexahedral elements of approximately $10 \times 10 \times 10$ mm³ size. The solid block is discretized with rigid (non-deformable) elements which have the same size with the Eulerian mesh elements in order to assure a proper description of the fluid-structure interaction (mesh compatibility). For more details, we refer to [36].

The numerical analyses account for diffraction and rarefaction phenomena, multiple reflections, non-normal incident angle of the blast waves with all the faces of the rocking block, and the three-dimensionality of the shock front. For example, due to diffraction, a rarefaction wave is developed when the shock front arrives at the boundaries of the impinged surface, while the diffracted wave continues to propagate on the rear surface. These effects result in an overall reduction of the blast impulse with respect to the analytical model. Nevertheless, this reduction is small.

The detailed numerical analyses showed limited uplifting even for combinations of stand-off distance and

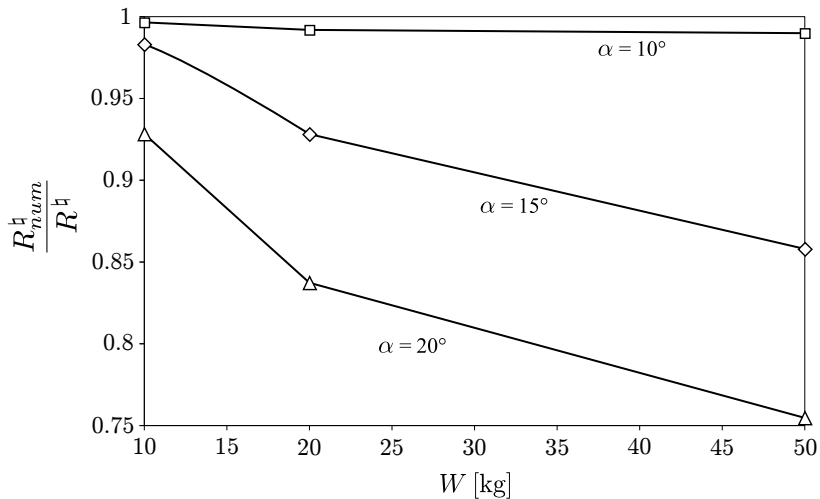


Figure 11: Ratio of the numerical overturning domain, R_{num}^{\natural} , and the analytical one, R^{\natural} , (cf. Tab. 1). The rocking block has $h = 1$ m, $\rho = 2000$ kg/m³ and variable slenderness angle α . Good agreement is found between the analytical model and the detailed numerical one. In the worst case study, the analytical model overestimates the minimum stand-off distance by approximately 25% (safety side).

explosive weight close to the critical ones. Therefore, the hypothesis of neglecting uplifting (flight modes) is justified and pertinent.

Despite the aforementioned phenomena that our simplified approach neglects, a remarkably good agreement of the numerical results with the analytical model is found. Table 2 presents the critical distance, as obtained from the numerical simulations, R_{FSI}^{\natural} , for slenderness $\alpha = 15^\circ$ and $W = 10, 20, 50$ kg. In Figure 13, we plot the ratio $R_{FSI}^{\natural}/R^{\natural}$ as function of W and we compare it with the one of C1 ($R_{num}^{\natural}/R^{\natural}$). An opposite trend is observed for increasing W . More specifically, the error of the simplified model is higher for small values of W and lower for large W . This difference is attributed to the aforementioned complex phenomena and depends on the geometry of the rocking object (cf. statues). Nevertheless, our simplified solution gives a safe estimate for the critical stand-off distance (upper bound) that it is close to the one derived from the detailed analysis. This means that the most important physics of the system are incorporated in our model and justifies the assumptions made in Section 2.

Table 2: Comparison of the overturning domain between the analytical solution, R^{\natural} , and the numerical one, R_{FSI}^{\natural} . The rocking block has $h = 1$ m, $\rho = 2000$ kg/m³, and slenderness angle $\alpha = 15^\circ$. Different weights of TNT, W , are considered. Again, good agreement is found, justifying the simplifying assumptions of the analytical model, which gives close upper bound estimates for the critical stand-off distance.

		$\alpha = 15^\circ$		
W	[kg]	10	20	50
R^{\natural}	[m]	1.88	2.53	3.67
R_{num}^{\natural}	[m]	1.50	2.25	3.35
$\frac{R_{num}^{\natural}}{R^{\natural}}$		0.7978	0.8893	0.9128

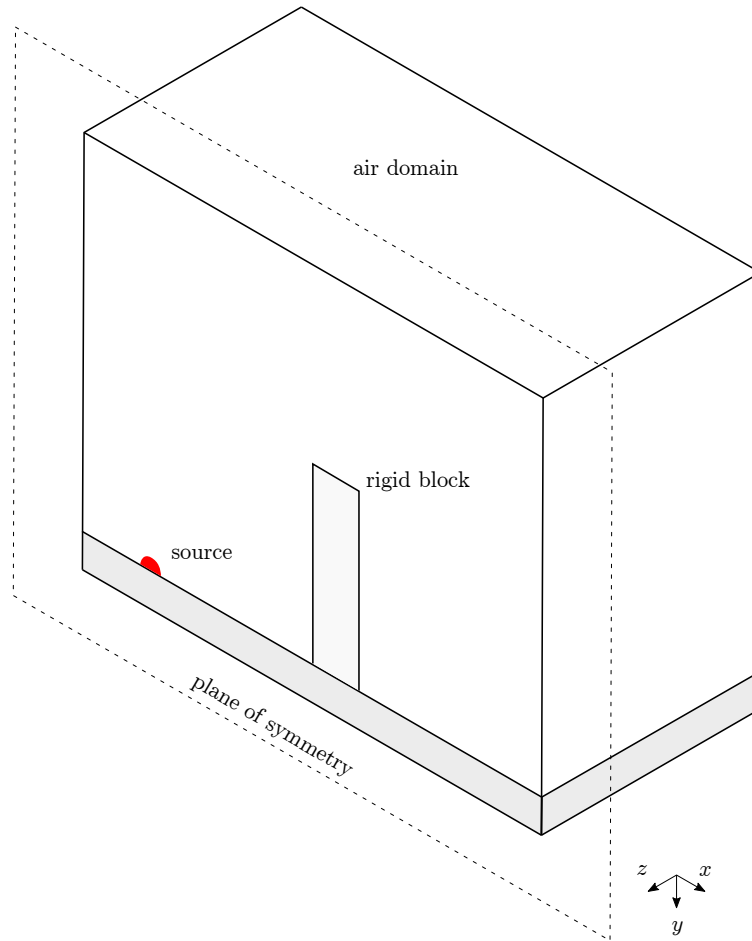


Figure 12: Geometrical domain used in the Finite Element numerical simulations, which consider three-dimensional Fluid-Structure Interaction between the target (in gray) and the blast waves originated by the detonation of the explosive source (in red).

5.3. Comparison C3

We investigate the reliability of the analytical model in predicting the rocking response and overturning of targets on the basis of the experimental tests conducted by Soper [17] and Scherbatiuk [12].

5.3.1. Soper's experimental tests

Soper (see also Baker et al. [37]) conducted tests of a prototype ten-wheel van subjected to the detonation of 226.8 kg (500 lb) TNT equivalent charge at a distance equal to 10.7 m (35 ft). Soper further examined a scaled model in which the geometry of the specimen, as well as the stand-off distance, were reduced by a factor of 20, requiring the invariance of the scaled distance Z . Table 3 presents the overall dimensions of the targets. Subscripts p and m refer to the prototype and the scaled model, respectively.

In both tests, the target showed a combined sliding/rocking response and overturned. However, no information is available about the time evolution of the rocking response in the experiments.

To compare our model, we consider a homogeneous rigid block with overall dimensions equal to those of the experiment (see Tab. 3) and same weight, imposing an equivalent density for the different widths (here denoted with subscripts f and b for front and back width, respectively). It is with no doubt that this

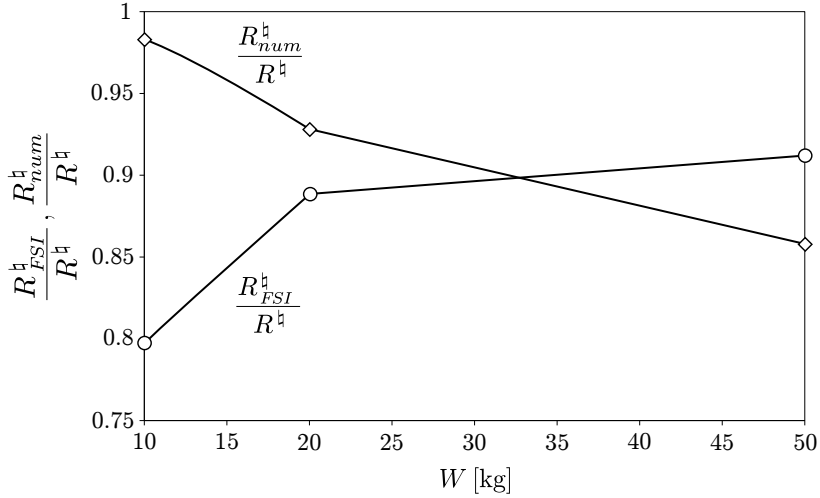


Figure 13: Ratio of the numerical overturning domains, R_{num}^h and R_{FSI}^h , and the analytical one, R^h , for a rocking block with $h = 1$ m, $\rho = 2000$ kg/m³, and slenderness $\alpha = 15^\circ$. Different weights of TNT, W , are considered and good agreement is found. The analytical solution provides safe estimates, with a maximum difference of 20%

is a strong simplification as *a*) we neglect the vehicle’s suspensions and *b*) we consider the geometric centre instead of the mass centroid of the van, which is lower due to the presence of the engine, the car shaft and the chassis. The latter assumption is justified by the fact that even though a lower centre of mass results in a decrease of the slenderness, the applied overturning moment due to the blast loading is higher (surface S remains unchanged, see Fig. 1), which counterbalances the effect of the lower mass centre (see Tab. 3).

The analytical model predicts for the prototype a critical stand-off distance $R_{fp}^h = 11.82$ m, considering the block’s width equal to the van’s front width, and $R_{bp}^h = 11.85$ m, for the back width.

For the scaled model, we obtain $R_{fm}^h = 1.072$ m and $R_{bm}^h = 1.073$ m, leading to overturning as in the experimental tests.

5.3.2. Scherbatiuk’s experimental tests

Scherbatiuk [12] investigated experimentally the response under explosive loads of free-standing soil-filled containers. He also developed two models for studying the rocking behaviour of the aforementioned soil-filled containers. The first one is a rocking rigid-body model, where the blast loading is considered only through an initial angular velocity applied at the block, while the second, called *rigid-body hybrid model*, goes further by accounting for the local deformation of the block at its pivot point. Both rigid and hybrid models were developed for non-slender structures (no-linearisation of the equation of motion) and they were integrated numerically in order to assess overturning. The numerical results were compared then with full-scale experiments. Here we refer only to trials 1, 4, and 6 (see [12], pp. 102-118), as the rest were for blocks with high slenderness angles ($\alpha \approx 58^\circ$), whose study exceeds the scope of the present work.

In Table 4 we compare the predictions of our model with the ones from [12] and the experimental results as far it concerns overturning. We recall that our model does not account for the deformability of the blocks tested and, therefore, it ignores the experimentally energy dissipation due to damage at the incident surface and the deformation of the block at the pivot point. Therefore, we expect to overestimate overturning, which results in a safety factor for applications and design. Moreover, our analytical model is valid only for slender blocks (i.e., $\alpha \lesssim 20^\circ$), while the targets in trials 1, 4, and 6 have a slenderness angle $\alpha = 31.61^\circ$. This means that our predictions underestimate the resistance to overturn, see Eq. (18), being again on the safety side. This is clearly shown in the comparison for trial 1, see Tab. 4. However, if the linearisation assumption is neglected and the non-linear equations of motion (10) are numerically integrated we do not

Table 3: Geometric parameters, explosive, and stand-off distance for the prototype and scaled model in [17], and corresponding parameters for the analytical model. Subscripts p and m refer to the prototype and the model test, respectively. Subscript f indicates that the rectangular rigid model has a width equal to the front width of the van, and subscript b to the back. Good agreement is found regarding overturning.

Experimental test							
Prototype			Scaled model				
<i>Front width</i>	1.77	m	$W_p = 226.8$ kg	<i>Front width</i>	88.39 mm	$W_m = 28.35$ g	
<i>Back width</i>	2.16	m	$R_p = 10.7$ m	<i>Back width</i>	108.2	mm	$R_m = 535$ mm
<i>Length</i>	5.85	m		<i>Length</i>	293.37	mm	
<i>Height</i>	2.93	m		<i>Height</i>	146.56	mm	
<i>Weight</i>	5443	kg		<i>Weight</i>	28.35	g	
Overturning : Y			Overturning : Y				
Analytical model							
Prototype			Scaled model				
$2b_{fp} = 1.77$ m			$W_p = 226.8$ kg	$2b_{fm} = 88.39$ mm		$W_m = 28.35$ g	
$2b_{bp} = 2.16$ m			$R_p = 10.7$ m	$2b_{bm} = 108.2$ mm		$R_m = 535$ mm	
$2h_p = 2.93$ m				$2h_m = 146.56$ mm			
$\rho_{fp} = 179.80$ kg/m ³				$\rho_{fm} = 179.80$ kg/m ³			
$\rho_{bp} = 7.46$ g/m ³				$\rho_{bm} = 6.09$ kg/m ³			
Overturning : Y			Overturning: Y				

have overturning in trial 1 and we predict a maximum rotation angle $\theta_{\max} = 17.7^\circ$ which is very close to the experimental results and closer than the prediction of Scherbatiuk hybrid model.

For trials 4 and 6, we present in Figure 14 the evolution of the horizontal block displacements as reported in [12]. The response of the experimental system is bounded by the linearised system (upper bound) and the non-linear one (lower bound).

Despite the complex physics involved (fluid-structure interaction phenomena, induced ground shocks vibration, etc.), the deformability of targets, and a combined rocking/sliding response of soil-filled containers subjected to explosions, our predictions exhibit good agreement with the experiment reality, on the safety side. They always provide a close upper bound of the critical stand-off distance for overturning.

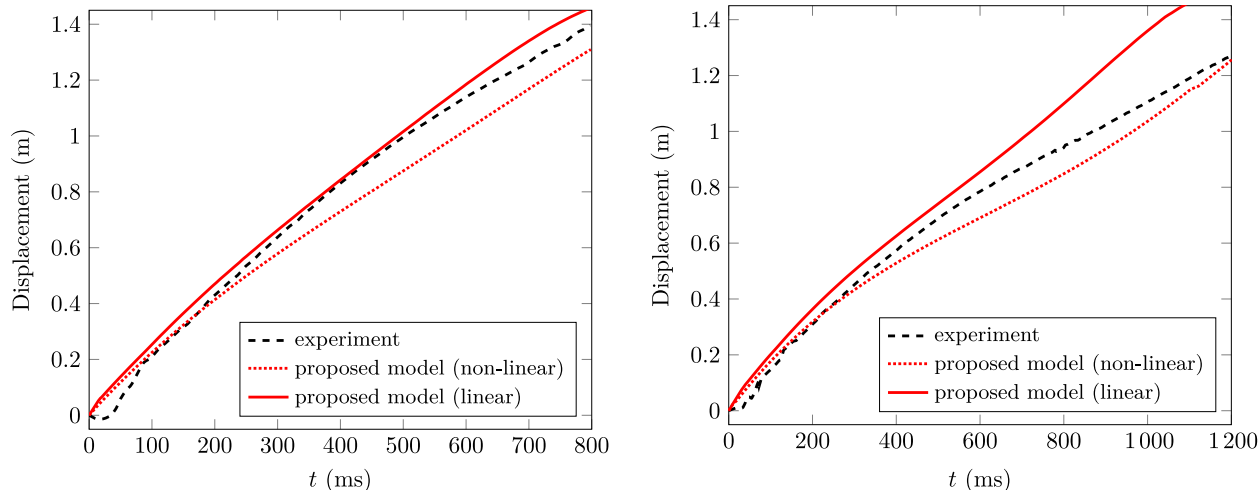


Figure 14: Comparison between the experimental results for trials 4 (left) and 6 (right) and the proposed analytical model in terms of the horizontal displacement of a point located at 1.50 m above the ground and on the rear face of the container. Both the linearised and non-linearised versions of the model, with respect to slenderness, are presented. The experimental response is closely bounded by the linearised system (upper bound) and the non-linear one (lower bound).

Table 4: Comparison between experimental tests [12], the rocking block models proposed by Scherbatiuk and our model. Targets dimensions are $1.2 \times 1.95 \times 3.9$ m ($2b \times 2h \times \text{depth}$). θ_{\max} represents the maximum rotation angle. Compared to previous analyses, our approach shows closer agreement regarding overturning and maximum inclination angle with the experimental results.

Trial	Blast impulse	Overturning (Y/N)				
		Experiment	Scherbatiuk models [12]		Proposed models	
			Rigid body model	Hybrid model	Analytical	Non-linear
1	$i_r = 4.096$ MPa.ms	N	N	N	Y	N
		$(\theta_{\max} = 15^\circ)$	$(\theta_{\max} = 13^\circ)$	$(\theta_{\max} = 20^\circ)$	–	$(\theta_{\max} = 17.7^\circ)$
4	$i_r = 4.184$ MPa.ms	Y	Y	Y	Y	Y
6	$i_r = 3.391$ MPa.ms	Y	N	Y	Y	Y

6. Concluding remarks

We investigated the dynamics of inverted pendulum structures under fast-dynamic excitations arising from an explosion. The purpose of our analysis is to derive reliable decision making tools in the design of protective devices to preserve the historical heritage, secure buildings and human beings.

First, by virtue of a simplified expression of blast actions and based on established empirical models, we derived the equations of motion for the rocking of inverted pendulum structures and analytical solutions for slender ones. In particular, it was found that the response is fully described by three non-dimensional parameters: the dimensionless rocking moment, χ , i.e., the ratio between the moment due to the blast load and the restoring moment due to gravity; the dimensionless load duration τ_o ; and d , the exponential decay coefficient used to model the decrease in time of the pressure resulting from an explosion. We derived then the overturning condition relying on an energy approach and we recovered the overturning strength in terms of the minimum distance (critical stand-off distance) that has to be assured between the explosive source and the target, such that toppling is avoided.

The stabilizing effect of the negative phase was investigated in order to provide more realistic estimations. In a similar manner, we derived a closed-form solution for the motion that depends on two additional dimensionless parameters. These are the dimensionless blast stabilising moment $\bar{\chi}$ and the dimensionless negative phase duration τ_{o-} . It is shown that the negative phase has a non-negligible impact and has to be taken into account.

Finally, the adequacy of the assumptions made to derive the analytical solutions of the rocking response and overturning domain of inverted pendulum structures was investigated through two set of numerical simulations and existing experimental tests.

The numerical solutions allowed to assess the effect of sliding and of the complex loading due to an explosion as well as the validity of the linearisation of the system. A good agreement was found. As expected, the analytical solution is exact for slender structures. For higher slenderness angles, α , the analytical computations overestimate to a small extent the critical distance, which from the design of point view favours safety. Fluid Structure Interaction simulations, performed with the well-established balloon analogue model, allowed to account for more complex behaviours (e.g. diffraction, rarefaction, multiple reflections, no-normal incidence, three-dimensional shock front, uplifting etc.). Again the estimations of the analytical model remain close to the numerical results and on the safety side. This means that the dominant features of the dynamic system are described by our analytical model.

The comparison of the proposed model with existing experimental tests of different target typologies showed good agreement and eventually validated our modelling assumptions.

Based on our model, the critical stand-off distance can be easily calculated. Herein, we presented it in the form of design charts, which can be helpful in applications. For instance they can be used in museums, for determining the minimum perimeter around statues of high historical and aesthetic value or, in the frame of protection of existing buildings and assets, for the construction and positioning of blast wall and barriers. The presented model can be used as well for devising energy absorbing systems based on rocking. Our work can be extended in the future for studying systems with multiple degrees-of-freedom as it is done for instance in [38] and [39]. Finally, the analytical derivations of the overturning domain can also be used in the design of experiments involving prototypes in reduced scale.

Appendix A. Analytical interpolations for blast loading

The expressions for the blast parameters that determine the reflected pressure time-history due to a surface burst (explosion on or very close to the ground surface) are given below and presented in Figure 6. For more details we refer to [40, 41].

- normal reflected pressure peak P_{ro} :

$$P_{ro}(Z) = \left(1 + \frac{1}{2e^{10Z}}\right) \exp \left[2.0304 - 1.8036 \ln Z - 0.09293 \ln^2 Z - 0.8779 \sin(\ln Z) - 0.3603 \sin^2(\ln Z) \right]$$

- scaled and effective positive reflected impulse i_{rw} , i_r :

$$\begin{aligned} i_{rw}(Z, W) &= \exp \left[-0.110157 - 1.40609 \ln Z + 0.0847358 \ln^2 Z \right], \\ i_r(Z) &= W^{\frac{1}{3}} i_{rw}(Z, W) \end{aligned}$$

- scaled and effective arrival time t_{Aw} , t_A :

$$t_{Aw}(Z, W) = \begin{cases} \exp \left[-0.6847 + 1.4288 \ln Z + 0.0290 \ln^2 Z + 0.4108 \sin(\ln Z) \right] & \text{if } Z \geq 0.18 \text{ m/kg}^{1/3}, \\ 0.0315495 & \text{if } Z < 0.18 \text{ m/kg}^{1/3}, \end{cases}$$

$$t_A(Z) = W^{\frac{1}{3}} t_{Aw}(Z, W)$$

- scaled and effective positive duration time t_{ow} , t_o :

$$t_{ow}(Z, W) = \begin{cases} \exp \left[0.592 + 2.913 \ln Z - 1.287 \ln^2 Z - 1.788 \ln^3 Z + 1.151 \ln^4 Z + 0.325 \ln^5 Z - 0.383 \ln^6 Z + 0.090 \ln^7 Z - 0.004 \ln^8 Z - 0.0004 \ln^9 Z + 0.537 \cos^7 \left[1.032 (\ln Z - 0.859) \right] \right. \\ \left. \sinh \left[1.088 (\ln Z - 2.023) \right] \right] & \text{if } Z \geq 0.18 \text{ m/kg}^{1/3}, \\ 0.251703 & \text{if } Z < 0.18 \text{ m/kg}^{1/3}, \end{cases}$$

$$t_o(Z) = W^{\frac{1}{3}} t_{ow}(Z, W)$$

- reflected negative pressure peak P_{ro-} :

$$P_{ro-}(Z) = \left(0.0415 + \frac{1}{2e^{0.1449Z}}\right) \exp \left[-1.7850 - 0.1213 \ln Z - 0.0514 \ln^2 Z - 0.4083 \sin(\ln Z) - 0.3824 \sin^2(\ln Z) \right]$$

- scaled and effective negative duration time t_{ow-} , t_{o-} :

$$\begin{aligned} t_{ow-}(Z, W) &= \exp \left[2.4052 + 0.1177 \ln Z + 0.0312 \ln^2 Z - 0.0107 \ln^3 Z + 0.1092 \cos(\ln Z) \right], \\ t_{o-}(Z) &= W^{\frac{1}{3}} t_{ow-}(Z, W) \end{aligned}$$

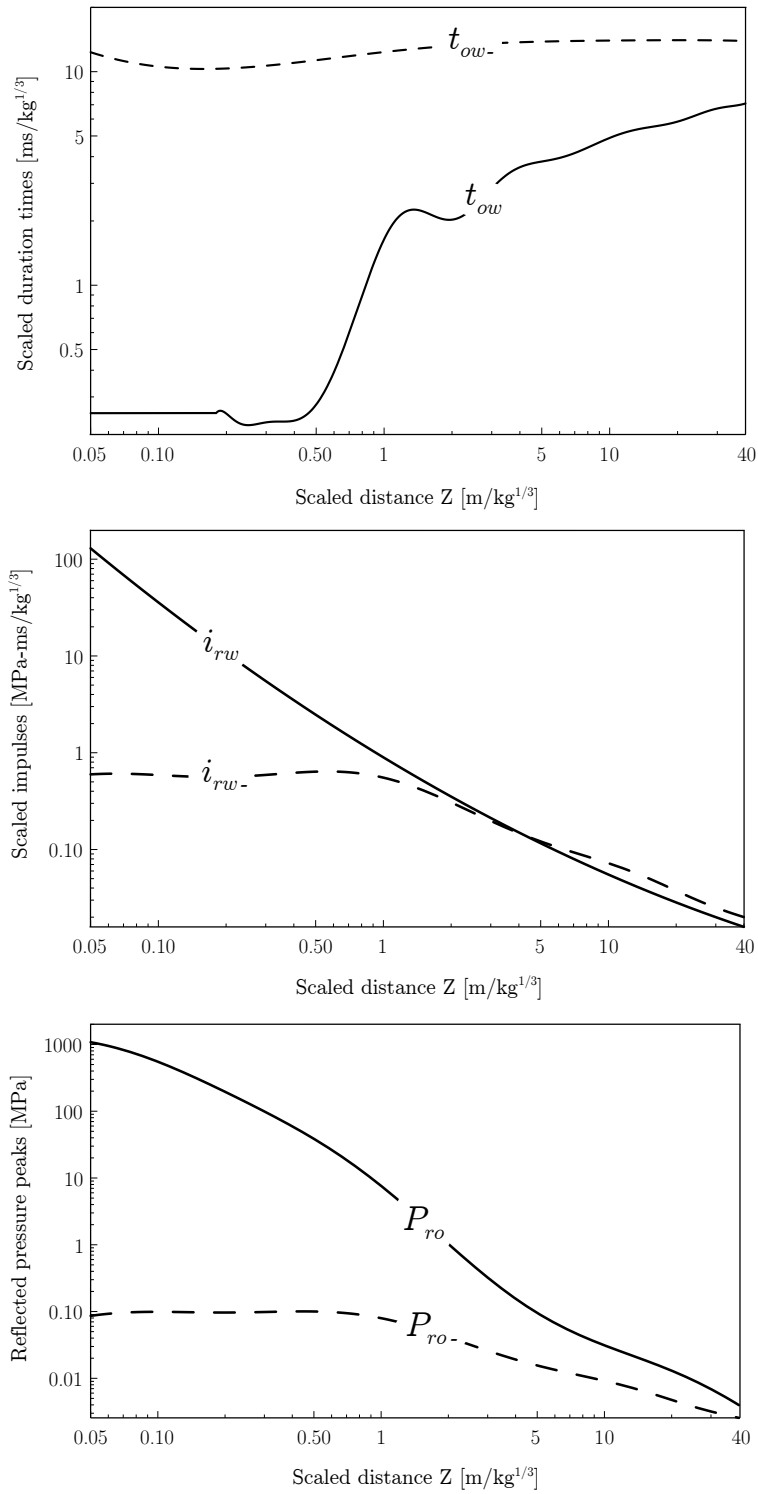


Figure 15: Analytical interpolations for blast loading: scaled duration times, impulses and reflected pressure as functions of the scaled distance, Z .

Appendix B. Analytical solutions of the equation of motion

B1. Positive phase

Analytical, closed-form solution of Equation (13): angular displacement, ϕ , and angular velocity, $\dot{\phi}$ (with $\zeta = d/\tau_o$).

$$\phi(\tau) = \begin{cases} \frac{\chi}{(\zeta^2-1)^2} \left\{ \begin{aligned} & \left[1 - \left(1 - \frac{2}{\tau_o}\right) \zeta \right] \cosh \tau + \\ & \left[\left(\zeta + \frac{1}{\tau_o}\right) (\zeta^2 - 1) - \frac{2}{\tau_o} \right] \sinh \tau - \\ & \left[(\zeta^2 - 1) (\zeta - 1) - 2\frac{\zeta}{\tau_o} \right] \cosh d\frac{\tau}{\tau_o} + \\ & \left[\frac{\tau}{\tau_o} (\zeta^2 - 1) - \left(\zeta - \frac{2}{\tau_o}\right) \zeta + 1 \right] \sinh d\frac{\tau}{\tau_o} \end{aligned} \right\} & \text{if } \tau \leq \tau_o, \\ \frac{1}{\tau_o} \frac{1}{(\zeta^2-1)^2} \left\{ \begin{aligned} & \left[(\zeta^2 + 1) e^{-\zeta\tau_o} \right] \chi \sinh \tau - \\ & \left[\zeta (\tau_o + \zeta - \zeta^2\tau_o) + 1 \right] \chi \sinh(\tau + \tau_o) - \\ & \left[(\zeta^2 - 1) \tau_o (\zeta^2 + \chi - 1) - 2\zeta\chi \right] \cosh(\tau + \tau_o) - \\ & 2\zeta\chi e^{-\zeta\tau_o} \cosh \tau \end{aligned} \right\} + 1 & \text{if } \tau > \tau_o. \end{cases}$$

$$\dot{\phi}(\tau) = \begin{cases} \frac{\chi}{(\zeta^2-1)^2} \left\{ \begin{aligned} & \left[1 + \left(1 - \frac{2}{\tau_o}\right) \zeta \right] \cosh \tau + \\ & \left[\left(\zeta + \frac{1}{\tau_o}\right) (\zeta^2 - 1) - \frac{2}{\tau_o} \right] \sinh \tau - \\ & \left[(\zeta^2 - 1) (\zeta - 1) + 2\frac{\zeta}{\tau_o} \right] \cosh d\frac{\tau}{\tau_o} + \\ & \left[\frac{\tau}{\tau_o} (\zeta^2 - 1) - \left(\zeta - \frac{2}{\tau_o}\right) \zeta + 1 \right] \sinh d\frac{\tau}{\tau_o} \end{aligned} \right\} & \text{if } \tau \leq \tau_o, \\ \frac{1}{\tau_o} \frac{1}{(\zeta^2-1)^2} \left\{ \begin{aligned} & \left[(\zeta^2 + 1) e^{-\zeta\tau_o} \cosh \tau + 2\zeta^2 e^{-\zeta\tau} \cosh \tau \right] \chi - \\ & \left[\zeta (\tau_o + \zeta - \tau_o\zeta^2) + 1 \right] \chi \cosh(\tau + \tau_o) - \\ & \left[(\zeta^2 - 1) \tau_o (\zeta^2 + \chi - 1) - 2\zeta\chi \right] \sinh(\tau + \tau_o) - \\ & 2\zeta\chi e^{-\zeta\tau} \sinh \tau \end{aligned} \right\} & \text{if } \tau > \tau_o. \end{cases}$$

B2. Positive and negative phase

Analytical, closed-form solution of Equation (20): angular displacement, ϕ , and angular velocity, $\dot{\phi}$.

$$\phi(\tau) = \left\{ \begin{array}{l} \frac{\chi}{(\zeta^2-1)^2} \left\{ \left[1 - \left(1 - \frac{2}{\tau_o} \right) \zeta \right] \cosh \tau + \left[\left(\zeta + \frac{1}{\tau_o} \right) (\zeta^2 - 1) - \frac{2}{\tau_o} \right] \sinh \tau - \right. \\ \left. \left[(\zeta^2 - 1) (\zeta - 1) - 2\frac{\zeta}{\tau_o} \right] \cosh d\frac{\tau}{\tau_o} + \left[\frac{\tau}{\tau_o} (\zeta^2 - 1) - \left(\zeta - \frac{2}{\tau_o} \right) \zeta + 1 \right] \sinh d\frac{\tau}{\tau_o} \right\} \\ \text{if } \tau \leq \tau_o, \\ \\ \frac{27\bar{\chi}}{4\tau_o^3} \left\{ \left[\tau^3 - \tau^2(3\tau_o + 2\tau_{o-}) + \tau[(\tau_o + \tau_{o-})(3\tau_o + \tau_{o-}) + 6] - \tau_o[(\tau_o + \tau_{o-})^2 + 6] - 4\tau_{o-} \right] + \right. \\ \left. \left[\tau_o((\tau_o + \tau_{o-})^2 + 6) + 4\tau_{o-} \right] \cosh \tau - \left[(\tau_o + \tau_{o-})(3\tau_o + \tau_{o-}) + 6 \right] \sinh \tau \right\} - \\ \frac{1}{\tau_o} \frac{1}{(\zeta^2-1)^2} \left\{ \left[(\zeta^2 - 1) \tau_o (\zeta^2 + \chi - 1) - 2\zeta\chi \right] \cosh(\tau + \tau_o) - \chi e^{-\zeta\tau_o} \left[(\zeta^2 + 1) \sinh \tau - 2\zeta \cosh \tau \right] - \right. \\ \left. \left[(\zeta^2 - 1) \zeta \tau_o - \zeta^2 - 1 \right] \chi \sinh(\tau + \tau_o) \right\} + 1 \\ \text{if } \tau_o < \tau \leq \tau_o + \tau_{o-}, \\ \\ \frac{1}{4(\zeta^2-1)^2\tau_o\tau_{o-}^3} \left\{ 54 (\zeta^2 - 1)^2 \tau_o\tau_{o-}\bar{\chi} \cosh \tau + 4 (\zeta^2 - 1)^2 \tau_o\tau_{o-}^3 + \right. \\ \left[27 (\zeta^2 - 1)^2 \tau_o\bar{\chi} [\tau_o((\tau_o + \tau_{o-})^2 + 6) + 4\tau_{o-}] - 8\zeta\tau_{o-}^3\chi e^{-\zeta\tau_o} \right] \cosh(\tau + \tau_o + \tau_{o-}) - \\ 4\tau_{o-}^3 \left[(\zeta^2 - 1) \tau_o (\zeta^2 + \chi - 1) - 2\zeta\chi \right] \cosh(\tau + 2\tau_o + \tau_o) + \\ 4 (\zeta^2 + 1) \tau_{o-}^3 \chi e^{-\zeta\tau_o} \sinh(\tau + \tau_o + \tau_{o-}) - \\ 27 (\zeta^2 - 1)^2 \tau_o\bar{\chi} \left[[(\tau_o + \tau_{o-})(3\tau_o + \tau_{o-}) + 6] \sinh(\tau + \tau_o + \tau_{o-}) - 6 \sinh \tau \right] - \\ 4\tau_{o-}^3 \chi \left[\zeta (\tau_o + \zeta - \zeta^2\tau_o) + 1 \right] \sinh(\tau + 2\tau_o + \tau_{o-}) \left. \right\} \\ \text{if } \tau > \tau_o + \tau_{o-}. \end{array} \right.$$

$$\dot{\phi}(\tau) = \left\{ \begin{array}{l}
\frac{\chi}{(\zeta^2-1)^2} \left\{ \left[1 + \left(1 - \frac{2}{\tau_o} \right) \zeta \right] \cosh \tau + \left[\left(\zeta + \frac{1}{\tau_o} \right) (\zeta^2 - 1) - \frac{2}{\tau_o} \right] \sinh \tau - \right. \\
\left. \left[(\zeta^2 - 1) (\zeta - 1) + 2 \frac{\zeta}{\tau_o} \right] \cosh d \frac{\tau}{\tau_o} + \left[\frac{\tau}{\tau_o} (\zeta^2 - 1) - \left(\zeta - \frac{2}{\tau_o} \right) \zeta + 1 \right] \sinh d \frac{\tau}{\tau_o} \right\} \\
\text{if } \tau \leq \tau_o, \\
\\
\frac{27\bar{\chi}}{4\tau_{o-}^3} \left\{ \left[3\tau^2 - 2\tau(3\tau_o + 2\tau_{o-}) + (\tau_o + \tau_{o-})(3\tau_o + \tau_{o-}) + 6 \right] - \right. \\
\left. \left[(\tau_o + \tau_{o-})(3\tau_o + \tau_{o-}) + 6 \right] \cosh \tau + \left[4\tau_{o-} + \tau_o(6 + (\tau_o + \tau_{o-})^2) \right] \sinh \tau \right\} - \\
\frac{1}{\tau_o} \frac{1}{(\zeta^2-1)^2} \left\{ \left[(\zeta^2 - 1) \zeta \tau_o - \zeta^2 - 1 \right] \chi \cosh(\tau + \tau_o) + \chi e^{-\zeta\tau_o} \left[(1 + \zeta^2) \cosh \tau - 2\zeta \sinh \tau \right] - \right. \\
\left. \left[(\zeta^2 - 1) \tau_o (\zeta^2 + \chi - 1) - 2\zeta\chi \right] \sinh(\tau + \tau_o) \right\} + 1 \\
\text{if } \tau_o < \tau \leq \tau_o + \tau_{o-}, \\
\\
\frac{1}{4(\zeta^2-1)^2\tau_o\tau_{o-}^3} \left\{ 4(\zeta^2 + 1) \tau_{o-}^3 \chi e^{-\zeta\tau_o} \cosh(\tau + \tau_o + \tau_{o-}) - \right. \\
27(\zeta^2 - 1)^2 \tau_o \bar{\chi} \left[\left[(\tau_o + \tau_{o-})(3\tau_o + \tau_{o-}) + 6 \right] \cosh(\tau + \tau_o + \tau_{o-}) - 6 \cosh \tau \right] - \\
4\tau_{o-}^3 \chi \left[\zeta (\tau_o + \zeta + -\zeta^2\tau_o) + 1 \right] \cosh(\tau + 2\tau_o + \tau_{o-}) + 54(\zeta^2 - 1)^2 \tau_o \tau_{o-} \bar{\chi} \sinh \tau + \\
\left[27(\zeta^2 - 1)^2 \tau_o \bar{\chi} \left[\tau_o \left[(\tau_o + \tau_{o-})^2 + 6 \right] + 4\tau_{o-} \right] - 8\zeta\tau_{o-}^3 \chi e^{-\zeta\tau_o} \right] \sinh(\tau + \tau_o + \tau_{o-}) - \\
4\tau_{o-}^3 \left[-2\zeta\chi + (-1 + \zeta^2)\tau_o(-1 + \zeta^2 + \chi) \right] \sinh(\tau + 2\tau_o + \tau_{o-}) \left. \right\} \\
\text{if } \tau > \tau_o + \tau_{o-}.
\end{array} \right.$$

References

- [1] N. Makris, D. Konstantinidis, [The rocking spectrum and the limitations of practical design methodologies](#), *Earthquake Engineering & Structural Dynamics* 32 (2) (2003) 265–289. doi:10.1002/eqe.223. URL <http://doi.wiley.com/10.1002/eqe.223>
- [2] F. Omori, Seismic experiments on the fracturing and overturning of columns, *Publications of the Earthquake Investigation Committee in Foreign Language* 4 (1900) 69–141.
- [3] F. Omori, On the overturning and sliding of columns, *Publications of the Earthquake Investigation Committee in Foreign Language* 12 (1902) 8–27.
- [4] G. W. Housner, [The behavior of inverted pendulum structures during earthquakes](#), *Bulletin of the seismological society of America* 53 (2) (1963) 403–417. URL <http://resolver.caltech.edu/CaltechAUTHORS:20140801-112753969>
- [5] J. Zhang, N. Makris, Rocking response of free-standing blocks under cycloidal pulses, *Journal of Engineering Mechanics* 127 (5) (2001) 473–483. doi:10.1061/(ASCE)0733-9399(2001)127:5(473).
- [6] E. Voyagaki, I. N. Psycharis, G. Mylonakis, Rocking response and overturning criteria for free standing rigid blocks to single-lobe pulses, *Soil Dynamics and Earthquake Engineering* 46 (2013) 85–95. doi:https://doi.org/10.1016/j.soildyn.2012.11.010.
- [7] E. G. Dimitrakopoulos, M. J. DeJong, Revisiting the rocking block: closed-form solutions and similarity laws, *Proceedings of the Royal Society of London A: Mathematical, Physical and Engineering Sciences* 468 (2144) (2012) 2294–2318. doi:10.1098/rspa.2012.0026.
- [8] F. Peña, F. Prieto, P. B. Lourenço, A. Campos Costa, J. V. Lemos, [On the dynamics of rocking motion of single rigid-block structures](#), *Earthquake Engineering & Structural Dynamics* 36 (15) 2383–2399. arXiv:https://onlinelibrary.wiley.com/doi/pdf/10.1002/eqe.739, doi:10.1002/eqe.739. URL <https://onlinelibrary.wiley.com/doi/abs/10.1002/eqe.739>
- [9] D. Konstantinidis, N. Makris, [Experimental and analytical studies on the response of 1/4-scale models of freestanding laboratory equipment subjected to strong earthquake shaking](#), *Bulletin of Earthquake Engineering* 8 (6) (2010) 1457–1477. doi:10.1007/s10518-010-9192-8. URL <https://doi.org/10.1007/s10518-010-9192-8>
- [10] D. Merkle, M. Rochefort, C. Tuan, Equipment shock tolerance, Tech. Rep. F08635-88-C-0067, U. S. Air Force Civil Engineering Support Agency, Tyndall Air Force Base, Albuquerque, NM (1993).
- [11] H. Hao, Y. Zhou, Dynamic response of rigid blocks to simultaneous horizontal and vertical ground shock, *Advances in Structural Engineering* 15 (7) (2012) 1069–1082. arXiv:https://doi.org/10.1260/1369-4332.15.7.1069, doi:10.1260/1369-4332.15.7.1069.
- [12] K. D. Scherbatiuk, Analytical models for calculating the response of temporary soil-filled walls subjected to blast loading, Ph.D. thesis, Department of Civil Engineering - University of Manitoba, Winnipeg, Manitoba (2010).
- [13] Generation of a pressure-impulse diagram for a temporary soil wall using an analytical rigid-body rotation model, *International Journal of Impact Engineering* 35 (6) (2008) 530 – 539. doi:https://doi.org/10.1016/j.ijimpeng.2007.04.006.
- [14] K. Scherbatiuk, N. Rattanawangcharoen, [Experimental testing and numerical modeling of soil-filled container walls](#), *Engineering Structures* 30 (12) (2008) 3545 – 3554. doi:https://doi.org/10.1016/j.engstruct.2008.05.030. URL <http://www.sciencedirect.com/science/article/pii/S0141029608002162>
- [15] G. H. Custard, J. R. Thayer, [Target response to explosive blast. ad0715475](#), Tech. rep., Falcon Research and Development. U.S. Department of Defense (1970). URL <http://www.dtic.mil/dtic/tr/fulltext/u2/715475.pdf>
- [16] W. E. Baker, J. J. Kulesz, R. E. Ricker, R. L. Bessey, P. S. Westine, V. B. Parr, G. A. Oldham, [Workbook for predicting pressure wave and fragment effects of exploding propellant tanks and gas storage vessels. 19760012208](#), Tech. rep., NASA, United States (1975). URL <https://ntrs.nasa.gov/archive/nasa/casi.ntrs.nasa.gov/19760012208.pdf>
- [17] W. G. Soper, Modeling laws related to target vulnerability, Tech. Rep. T-9/67 (Classified), U. S. Naval Weapons Lab, Dahlgren, Virginia (1967).
- [18] L. Blanc, S. Santana Herrera, J. L. Hanus, Simulating the blast wave from detonation of a charge using a balloon of compressed air, *Shock Waves* 28 (4) (2018) 641–652. doi:10.1007/s00193-017-0774-0.
- [19] I. Stefanou, I. Vardoulakis, A. Mavraganis, Dynamic motion of a conical frustum over a rough horizontal plane, *International Journal of Non-Linear Mechanics* 46 (1) (2011) 114–124. doi:https://doi.org/10.1016/j.ijnonlinmec.2010.07.008.
- [20] Rocking and kinematic approaches for rigid block analysis of masonry walls: State of the art and recent developments, *Buildings* 7 (4) (2017) 69. doi:10.3390/buildings7030069.
- [21] C. Papadopoulos, E. Basanou, I. Vardoulakis, M. Boulon, G. Armand, Mechanical behaviour of Dionysos marble smooth joints under cyclic loading: II constitutive modelling, in: *Proceedings of the international conference on mechanics of jointed and faulted rock*, Vienna, Austria, 1998.
- [22] A. M. Remennikov, A review of methods for predicting bomb blast effects on buildings, *Journal of Battlefield Technology* 6 (2003) 5–10.
- [23] M. Larcher, F. Casadei, Explosions in Complex Geometries — A Comparison of Several Approaches, *International Journal of Protective Structures* 1 (2) (2010) 169–195. doi:10.1260/2041-4196.1.2.169.
- [24] J. M. Dewey, *Measurement of the Physical Properties of Blast Waves*, Springer International Publishing, Cham, 2016, pp. 53–86. doi:10.1007/978-3-319-23745-9_2.

- [25] C. N. Kingery, G. Bulmash, Technical report ARBRL-TR-02555: Air blast parameters from TNT spherical air burst and hemispherical burst, Tech. rep., U.S. Army Ballistic Research Laboratory (1984).
- [26] F. G. Friedlander, The diffraction of sound pulses. i. diffraction by a semi-infinite plate., *Proceedings of the Royal Society of London A* (186) (1946) 322 – 344.
- [27] S. A. Granström, Loading characteristics of air blasts from detonating charges, Tech. Rep. 100, Transactions of the Royal Institute of Technology, Stockholm (1956).
- [28] S. E. Rigby, A. Tyas, T. Bennett, S. D. Clarke, S. D. Fay, The negative phase of the blast load, *International Journal of Protective Structures* 5 (1) (2014) 1–19. doi:10.1260/2041-4196.5.1.1.
- [29] H. Jones, A. R. Miller, The detonation of solid explosives: the equilibrium conditions in the detonation wave-front and the adiabatic expansion of the products of detonation, *Proceedings of the Royal Society of London A: Mathematical, Physical and Engineering Sciences* 194 (1039) (1948) 480–507. doi:10.1098/rspa.1948.0093.
- [30] M. L. Wilkins, B. Squier, B. Halperin, The equation of state of PBX 9404 and LX-04-01, in: Tenth Symposium (International) on Combustion, (The Combustion Institute), 1965, pp. 769–778.
- [31] E. L. Lee, H. C. Hornig, J. W. Kury, Adiabatic Expansion Of High Explosive Detonation Products, 1968. doi:10.2172/4783904.
- [32] D. L. Chapman, On the rate of explosion in gases, *The London, Edinburgh, and Dublin Philosophical Magazine and Journal of Science* 47 (284) (1899) 90–104. doi:10.1080/14786449908621243.
- [33] E. Jouguet, On the propagation of chemical reactions in gases, *Journal de Mathematiques Pures et Appliquees* 1 (347–425) (1905) 2.
- [34] H. L. Brode, Numerical solutions of spherical blast waves, *Journal of Applied Physics* 26 (6) (1955) 766–775. doi:10.1063/1.1722085.
- [35] ABAQUS, Abaqus analysis user’s guide, Tech. Rep. Abaqus 6.14 Documentation, Simulia Corp. (2016).
- [36] F. Masi, I. Stefanou, P. Vannucci, A study on the effects of an explosion in the Pantheon of Rome, *Engineering Structures* 164 (2018) 259–273. doi:10.1016/j.engstruct.2018.02.082.
- [37] W. E. Baker, P. S. Westine, F. T. Dodge, *Simulating rigid body motion*, in: *Similarity Methods in Engineering Dynamics*, Vol. 12 of *Fundamental Studies in Engineering*, Elsevier, 1991, pp. 73 – 95. doi:https://doi.org/10.1016/B978-0-444-88156-4.50011-7.
URL <http://www.sciencedirect.com/science/article/pii/B9780444881564500117>
- [38] I. N. Psycharis, M. Fragiadakis, I. Stefanou, *Seismic reliability assessment of classical columns subjected to near-fault ground motions*, *Earthquake Engineering & Structural Dynamics* 42 (14) (2013) 2061–2079. doi:10.1002/eqe.2312.
URL <http://doi.wiley.com/10.1002/eqe.2312>
- [39] N. Makris, M. F. Vassiliou, *Planar rocking response and stability analysis of an array of free-standing columns capped with a freely supported rigid beam*, *Earthquake Engineering & Structural Dynamics* 42 (3) (2013) 431–449. arXiv:arXiv:1403.5481v1, doi:10.1002/eqe.2222.
URL <http://doi.wiley.com/10.1002/eqe.2222>
- [40] P. Vannucci, F. Masi, I. Stefanou, *A study on the simulation of blast actions on a monumental structure*.
URL <https://hal.archives-ouvertes.fr/hal-01447783v3/document>
- [41] F. Masi, Blast actions from high explosives. Studies on their simulation and effects, Master Thesis - Department of Mechanical Engineering - University of Florence, 2017. doi:10.17605/osf.io/ekus8.